Creating a False Memory in the Hippocampus

Steve Ramirez *et al.*

Science **341**, 387 (2013);
DOI: 10.1126/science.1239073

Science (print ISSN 0036-8075; online ISSN 1095-9203) is published weekly, except the last week in December, by the American Association for the Advancement of Science, 1200 New York Avenue NW, Washington, DC 20005.

In colony allorecognition assays, three of four isogenic pairs receiving control morpholinos fused within 24 hours of ampullae contact. By contrast, no reactions were observed in isogenic pairs receiving BHF translation-blocking morpholinos (n = 6), despite constant physical contact over observational periods ranging from 2 to 7 days (Fig. 3D, fig. S19, and table S8). To exclude nonspecific effects, we also tested *BHF* splice-inhibiting morpholinos, using the progeny of wild-type colonies (*15*). Within 2 days of ampullae contact, all control pairs had fused (n = 2) or rejected (n = 1), whereas colony pairs receiving splice-inhibiting morpholinos did not react (n = 5) (figs. S20 and S21, table S9, and movies S1 and S2). These data support our genomic analysis and indicate that BHF participates in fusion and rejection initiation.

In the jawed vertebrates, the MHC is a haplotype, each sublocus of which specifies a different recognition process, usually by unique subsets of cells (*18*–*20*). By contrast, the *B. schlosseri* Fu/HC locus is a single gene (*BHF*) embedded in a haplotype of several genes with high polymorphism. Unlike the secreted (*sFuHC*) and membrane-bound (*mFuHC*) genes, *BHF* has none of the domains expected for a cell surface–recognition protein or, in fact, domains that are conserved throughout protein evolution. Because *BHF* does not follow biological precedence by either sequence or domains, future investigations of this gene will likely reveal new mechanisms of recognition.

The ability to reliably predict histocompatibility outcomes on the basis of a single gene has broad implications for the study of allorecognition. For example, after vasculature fusion, stem cells from each *B. schlosseri* colony compete to overtake germline and/or somatic lineages (*21*–*24*). Stem cell competition may lead to elimination of the other colony's genome or may produce a chimeric colony with mixed genotypes. To date, induction of chimerism using hematopoietic stem-cell transplantation is the only way to achieve long-term donor-specific tolerance to human organ allografts (*25*). Chimerism can be short-lived, and if lost, the threat of allograft rejection emerges. *B. schlosseri* is a unique species for studying stem cell–mediated chimerism, and such research will be facilitated by BHF.

References and Notes

1. A. Nakashima, T. Shima, K. Inada, M. Ito, S. Saito, *Am. J. Reprod. Immunol.* **67**, 304 (2012).
2. G. Girardi, Z. Prohászka, R. Bulla, F. Tedesco, S. Scherjon, *Mol. Immunol.* **48**, 1621 (2011).
3. M. Colonna, S. Jonjic, C. Watzl, *Nat. Immunol.* **12**, 107 (2011).
4. D. F. LaRosa, A. H. Rahman, L. A. Turka, *J. Immunol.* **178**, 7503 (2007).
5. F. Delsuc, H. Brinkmann, D. Chourrout, H. Philippe, *Nature* **439**, 965 (2006).
6. H. Oka, H. Watanabe, *Proc. Jpn. Acad.* **33**, 657 (1957).
7. H. Oka, H. Watanabe, *Bull. Mar. Biol. Stat. Asamushi.* **10**, 153 (1960).
8. A. Sabbadin, *Rend. Accad. Naz. Lincei. Ser.* **32**, 1031 (1962).
9. V. L. Scofield, J. M. Schlumpberger, L. A. West, I. L. Weissman, *Nature* **295**, 499 (1982).
10. A. W. De Tomaso, Y. Saito, K. J. Ishizuka, K. J. Palmeri, I. L. Weissman, *Genetics* **149**, 277 (1998).
11. A. W. De Tomaso, I. L. Weissman, *Immunogenetics* **55**, 480 (2003).
12. A. W. De Tomaso *et al.*, *Nature* **438**, 454 (2005).
13. A. Voskoboynik *et al., eLife* **2**, e00569 (2013).
14. I. Letunic, T. Doerks, P. Bork, SMART 7: recent updates to the protein domain annotation resource. *Nucleic Acids Res.* **40**, D302 and (2012).
15. Materials and methods are available as supplementary materials on *Science* Online.
16. B. Rinkevich, J. Douek, C. Rabinowitz, G. Paz, *Dev. Comp. Immunol.* **36**, 718 (2012).
17. M. Oren, J. Douek, Z. Fishelson, B. Rinkevich, *Dev. Comp. Immunol.* **31**, 889 (2007).
18. The MHC sequencing consortium, *Nature* **401**, 921 (1999).
19. M. Hirano, S. Das, P. Guo, M. D. Cooper, *Adv. Immunol.* **109**, 125 (2011).
20. L. J. Dishaw, G. W. Litman, *Curr. Biol.* **19**, R286 (2009).
21. D. S. Stoner, I. L. Weissman, *Proc. Natl. Acad. Sci. U.S.A.* **93**, 15254 (1996).
22. D. S. Stoner, B. Rinkevich, I. L. Weissman, *Proc. Natl. Acad. Sci. U.S.A.* **96**, 9148 (1999).
23. D. J. Laird, A. W. De Tomaso, I. L. Weissman, *Cell* **123**, 1351 (2005).
24. A. Voskoboynik *et al.*, *Cell Stem Cell* **3**, 456 (2008).
25. D. H. Sachs, M. Sykes, T. Kawai, A. B. Cosimi, *Semin. Immunol.* **23**, 165 (2011).

Acknowledgments: We thank B. Rinkevich for pointing out the difficulty with the original cFuHC assignments and T. Snyder, J. Okamoto, L. Me, L. Ooi, A. Dominguez, C. Lowe, K. Uhlinger, L. Crowder, S. Karten, C. Patton, L. Jerabek, and T. Storm for invaluable technical advice and help. A. De Tomaso provided the fosmid sequence used to characterize *cFuHC* (*12*) (table S5). D.P., A.V., and S.R.Q. have filed U.S. and international patent applications (61/532,882 and 13/608,778, respectively) entitled "Methods for obtaining a sequence." This invention allows for the sequencing of long continuous (kilobase scale) nucleic acid fragments using conventional short read–sequencing technologies, useful for consensus sequencing and haplotype determination. This study was supported by NIH grants 1R56AI089968, R01GM100315, and 1R01AG037968 awarded to I.L.W., A.V., and S.R.Q., respectively, and the Virginia and D. K. Ludwig Fund for Cancer Research awarded to I.L.W. D.S. was supported by NIH grant K99CA151673-01A1 and Department of Defense Grant W81XWH-10-1-0500, and A.M.N., D.M.C., D.S., and I.K.D. were supported by a grant from the Siebel Stem Cell Institute and the Thomas and Stacey Siebel Foundation. The data in this paper are tabulated in the main manuscript and in the supplementary materials. BHF, sFuHC, and mFuHC sequences are available in GenBank under accession numbers KF017887-KF017889, and the RNA-Seq data are available on the Sequence Read Archive (SRA) database: BioProject SRP022042.

Supplementary Materials

www.sciencemag.org/cgi/content/full/341/6144/384/DC1
Materials and Methods
Figs. S1 to S21
Tables S1 to S9
References (*26*–*42*)
Movies S1 and S2

19 March 2013; accepted 30 May 2013
10.1126/science.1238036

Creating a False Memory in the Hippocampus

Steve Ramirez,[1]* Xu Liu,[1,2]* Pei-Ann Lin,[1] Junghyup Suh,[1] Michele Pignatelli,[1] Roger L. Redondo,[1,2] Tomás J. Ryan,[1,2] Susumu Tonegawa[1,2]†

Memories can be unreliable. We created a false memory in mice by optogenetically manipulating memory engram–bearing cells in the hippocampus. Dentate gyrus (DG) or CA1 neurons activated by exposure to a particular context were labeled with channelrhodopsin-2. These neurons were later optically reactivated during fear conditioning in a different context. The DG experimental group showed increased freezing in the original context, in which a foot shock was never delivered. The recall of this false memory was context-specific, activated similar downstream regions engaged during natural fear memory recall, and was also capable of driving an active fear response. Our data demonstrate that it is possible to generate an internally represented and behaviorally expressed fear memory via artificial means.

Neuroscience aims to explain how brain activity drives cognition. Doing so requires identification of the brain regions that are specifically involved in producing internal mental representations and perturbing their activity to see how various cognitive processes are affected. More specifically, humans have a rich repertoire of mental representations generated internally by processes such as conscious or unconscious recall, dreaming, and imagination (*1*, *2*). However, whether these internal representations can be combined with external stimuli to generate new memories has not been vigorously studied.

Damage to the hippocampus impairs episodic memory (*3*–*8*). Recently, using fear conditioning in mice as a model of episodic memory, we identified a small subpopulation of granule cells in the dentate gyrus (DG) of the hippocampus as contextual memory-engram cells. Optogenetic stimulation of these cells is sufficient to activate behavioral recall of a context-dependent fear memory formed by a delivery of foot shocks. This finding provided an opportunity to investigate how the internal representation of a specific context can be associated with external stimuli of high valence. In particular, a hypothesis of great interest is

[1]RIKEN–Massachusetts Institute of Technology (MIT) Center for Neural Circuit Genetics at the Picower Institute for Learning and Memory, Department of Biology and Department of Brain and Cognitive Sciences, MIT, Cambridge, MA 02139, USA. [2]Howard Hughes Medical Institute, MIT, Cambridge, MA 02139, USA.

*These authors contributed equally to this work.
†Corresponding author. E-mail: tonegawa@mit.edu

whether artificially activating a previously formed contextual memory engram while simultaneously delivering foot shocks can result in the creation of a false fear memory for the context in which foot shocks were never delivered. To address this, we investigated whether a light-activated contextual memory in the DG or CA1 can serve as a functional conditioned stimulus (CS) in fear conditioning.

Our system uses c-fos-tTA transgenic mice, in which the promoter of the *c-fos* gene drives the expression of the tetracycline transactivator (tTA) to induce expression of a gene of interest downstream of the tetracycline-responsive element (TRE) (*8*–*12*). We injected an adeno-associated virus (AAV) encoding TRE-ChR2-mCherry into the DG or CA1 of c-fos-tTA animals (Fig. 1A). Channelrhodopsin-2 (ChR2)–mCherry expression was completely absent in the DG of animals that had been raised with doxycycline (Dox) in the diet (on Dox) (Fig. 1B). Exploration of a novel context under the condition of Dox withdrawal (off Dox) elicited an increase in ChR2-mCherry expression (Fig. 1C). We confirmed the functionality of the expressed ChR2-mCherry by recording light-induced spikes in cells expressing ChR2-mCherry from both acute hippocampal slices and in anaesthetized animals (Fig. 1, D to F). Furthermore, optical stimulation of ChR2-mCherry–expressing DG cells induced cFos expression throughout the anterior-posterior axis of the DG (fig. S1, A to I).

We first took virus-infected and fiber-implanted animals off Dox to open a time window for labeling cells activated by the exploration of a novel context (context A) with ChR2-mCherry. The animals were then put back on Dox to prevent any further labeling. The next day, we fear-conditioned this group in a distinct context (context B) while optically reactivating the cells labeled in context A. On the following 2 days, we tested the animals' fear memory in either the original context A or a novel context C (Fig. 1G). If the light-reactivated cells labeled in context A can produce a functional CS during fear conditioning in context B, then the animals should express a false fear memory by freezing in context A, but not in context C.

First, we examined the degree of overlap of the cell populations activated in contexts A and C (*8*, *11*). We injected a group of c-fos-tTA mice with an AAV virus encoding TRE-ChR2-mCherry and exposed them to context A while off Dox so as to label activated DG cells with ChR2-mCherry. These animals were then immediately placed back on Dox to prevent further labeling. The next day, half of the animals were exposed to context C, and the other half were reexposed to context A as a control. Both groups were euthanized 1.5 hours later. DG cells activated by the first exposure to context A were identified by ChR2-mCherry expression, and cells activated by the exposure to context C or the reexposure to context A were identified by the expression of endogenous c-Fos. The c-Fos generated by the first exposure to context A had been degraded by the time the animals underwent their second context exposure (*11*). Contexts A and C recruited statistically independent populations of DG cells. In contrast, two exposures to context A recruited substantially overlapping cell populations in the dorsal DG (Fig. 2, A to E).

When DG cells activated by the exposure to context A were reactivated with light during fear conditioning in a distinct context B, the animals subsequently froze in context A at levels significantly higher than the background levels, whereas freezing in context C did not differ from background levels (Fig. 2F). This increased freezing in context A was not due to generalization, because a control group expressing only mCherry that underwent the exact same training protocol did not show the same effect (Fig. 2F). A separate group of animals expressing ChR2–enhanced yellow fluorescent protein

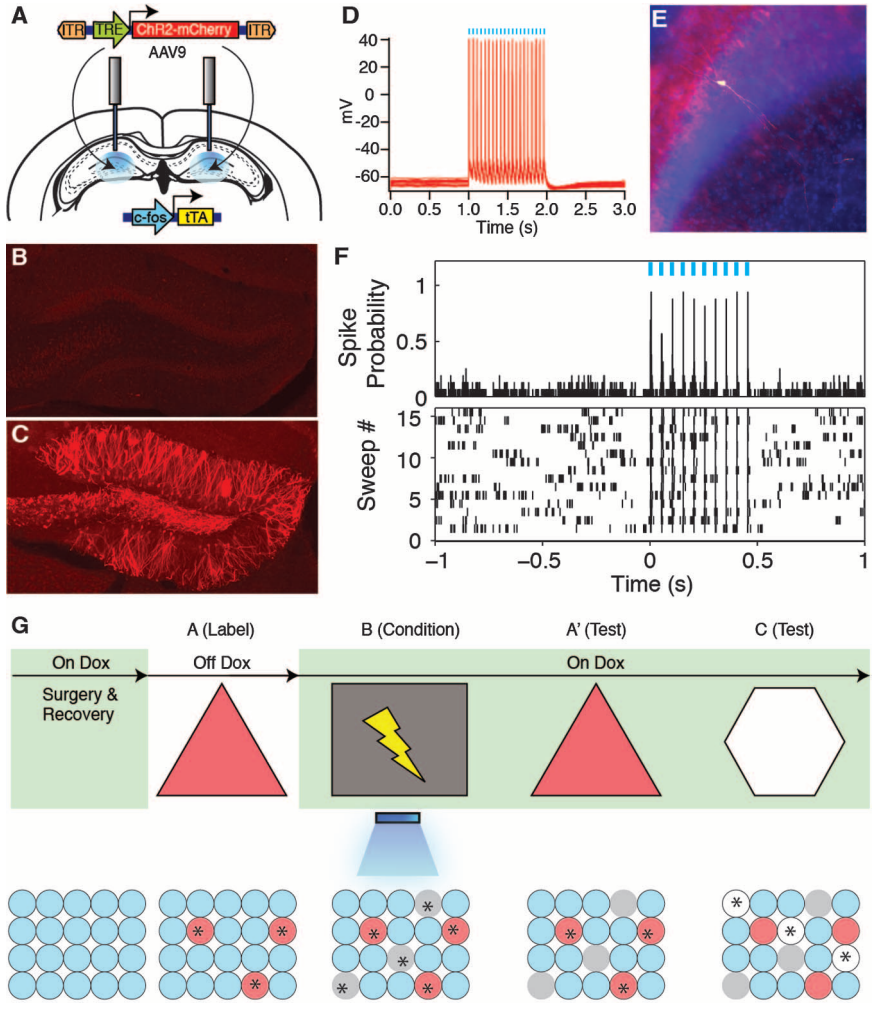

Fig. 1. Activity-dependent labeling and light-activation of hippocampal neurons, and the basic experimental scheme. (**A**) The c-fos-tTA mice were bilaterally injected with AAV_9-TRE-ChR2-mCherry and implanted with optical fibers targeting DG. (**B**) While on Dox, exploration of a novel context did not induce expression of ChR2-mCherry. (**C**) While off Dox, exploration of a novel context induced expression of ChR2-mCherry in DG. (**D**) Light pulses induced spikes in a CA1 neuron expressing ChR2-mCherry. The recorded neuron is shown labeled with biocytin in (**E**). (**F**) Light pulses induced spikes in DG neurons recorded from a head-fixed anesthetized c-fos-tTA animal expressing ChR2-mCherry. (**G**) Basic experimental scheme. Post-surgery mice were taken off Dox and allowed to explore context A in order to let DG or CA1 cells become labeled with ChR2-mCherry. Mice were put back on Dox and fear conditioned in context B with simultaneous delivery of light pulses. Freezing levels were then measured in both the original context A and a novel context C. The light green shading indicates the presence of Dox in the diet during corresponding stages of the scheme. Prime indicates the second exposure to a given context. The yellow lightning symbol and blue shower symbol indicate foot shocks and blue light delivery, respectively. Red circles represent neurons encoding context A that are thus labeled with ChR2-mCherry. Gray and white circles represent neurons encoding context B and C, respectively. Asterisks indicate neurons activated either by exposure to context or light stimulation.

(EYFP) instead of ChR2-mCherry in the DG that underwent the same behavioral schedule also showed increased freezing in context A (fig. S2A).

New experimental and control groups of mice were taken off Dox in context A in order to label activated cells and then placed in context C on the following day while back on Dox. In this experiment, although conditioning took place after the formation of both context A and context C memories, only those cells encoding context A were reactivated by light during fear conditioning. Subsequently, all groups of mice displayed background levels of freezing in context C. In contrast, in the context A test the next day, the experimental group showed increased freezing levels as compared with those of the mCherry-only group, confirming that the recall of the false memory is specific to context A (Fig. 2G). This freezing was not observed in another ChR2-mCherry group that underwent the same behavioral protocol but without light stimulation during fear conditioning in context B, or in a group in which an immediate shock protocol was administered in context B with light stimulation of context A cells (Fig. 2G and fig. S3). In a separate group of animals, we labeled cells active in context C rather than context A and repeated similar experiments as above. These animals showed freezing in context C but not context A (fig. S2B).

The hippocampus processes mnemonic information by altering the combined activity of subsets of cells within defined subregions in response to discrete episodes (*11*–*13*). Therefore, we investigated whether applying the same parameters and manipulations to CA1 as we did to the DG could form a false memory. We first confirmed that light could activate cells expressing ChR2-mCherry along the anterior-posterior axis of the CA1 similar to the DG (fig. S1, J to R). Also similar to the DG (Fig. 2, A to E), the overlap of active CA1 cells was significantly lower across contexts (A and C) as compared with that of a reexposure to the same context (A and A). However, the degree of overlap for the two contexts was much greater in CA1 (30%) than in the DG (~1%). When we labeled CA1 cells activated in context A and reactivated these cells with light during fear conditioning in context B, no increase in freezing was observed in the experimental group expressing ChR2-mCherry as compared with the mCherry-only control group in either context A or context C, regardless of whether the animals were exposed to context C or not before fear conditioning in context B (Fig. 2, M and N).

The simultaneous availability of two CSs can sometimes result in competitive conditioning; the memory for each individual CS is acquired less strongly as compared with when it is presented alone, and the presentation of two simultaneous CSs to animals trained with a single CS can also lead to decrement in recall (*14*). In our experiments, it is possible that the light-activated DG cells encoding context A interfered with the acquisition or expression of the genuine fear memory for context B. Indeed, upon reexposure to context B, the experimental group froze significantly less than the group that did not receive light during fear conditioning or the group expressing mCherry alone (Fig. 3A and fig. S4). During light-on epochs in the context B test, freezing increased in the experimental group and decreased in the group that did not receive light during fear conditioning (Fig. 3A and fig. S2C). We conducted similar experiments with mice in which the manipulation was targeted to the CA1 region and found no differences in the experimental or control groups during either light-off or light-on epochs of the context B test (fig. S5A).

Memory recall can be induced for a genuine fear memory by light reactivation of the corresponding engram in the DG (*8*). To investigate

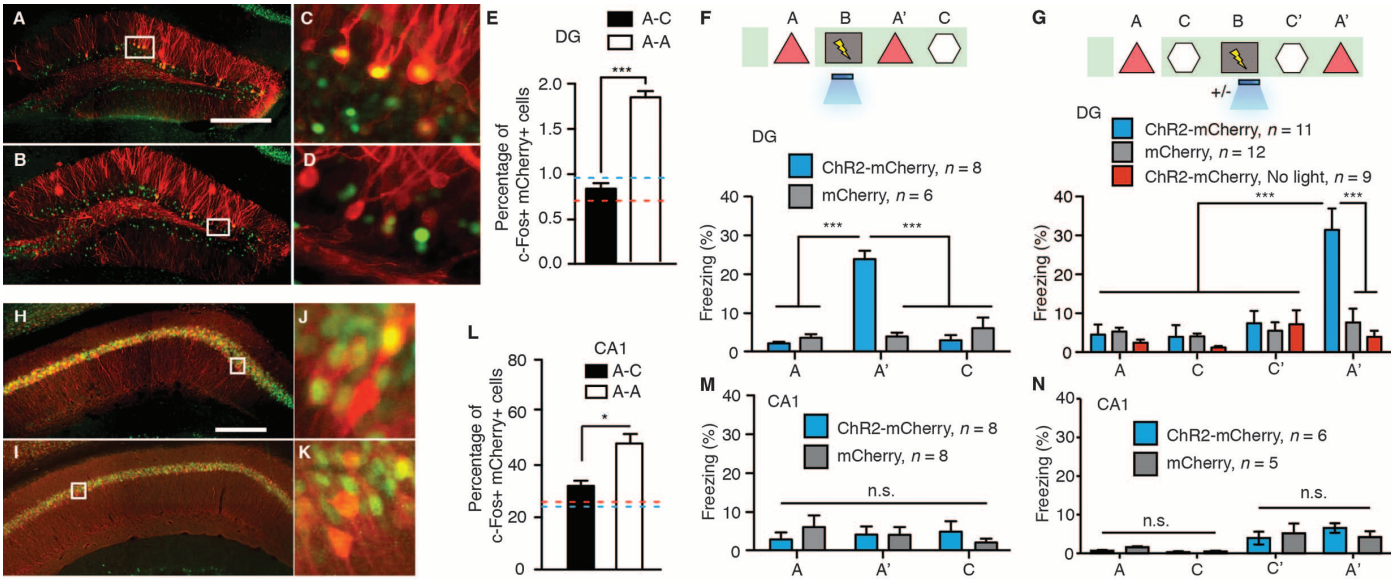

Fig. 2. Creation of a false contextual fear memory. (**A** to **E**) c-fos-tTA mice injected with AAV_9-TRE-ChR2-mCherry in the DG were taken off Dox and exposed to context A in order to label the activated cells with mCherry (red), then put back on Dox and exposed to the same context A [(A) and (C)] or a novel context C [(B) and (D)] 24 hours later so as to let activated cells express c-Fos (green). Images of the DG from these animals are shown in (A) to (D), and the quantifications are shown in (E) (n = 4 subjects each; ***P < 0.001, unpaired Student's t test). Blue and red dashed lines indicate the chance level of overlap for A-A and A-C groups, respectively. (**F**) (Top) Training and testing scheme of animals injected with AAV_9-TRE-ChR2-mCherry or AAV_9-TRE-mCherry. Various symbols are as explained in Fig. 1. (Bottom) Animals' freezing levels in context A before fear conditioning and in context A and C after fear conditioning [n = 8 subjects for ChR2-mCherry group, and n = 6 subjects for mCherry group; ***P < 0.001, two-way analysis of variance (ANOVA) with repeated measures followed by Bonferroni post-hoc test]. (**G**) (Top) Training and testing scheme of animals injected with AAV_9-TRE-ChR2-mCherry or AAV_9-TRE-mCherry. One control group injected with AAV_9-TRE-ChR2-mCherry did not receive light stimulation during fear conditioning (ChR2-mCherry, no light). (Bottom) Animals' freezing levels in context A and C before and after fear conditioning (n = 11 subjects for ChR2-mCherry group, n = 12 subjects for mCherry, and n = 9 subjects for ChR2-mCherry, no-light groups; ***P < 0.001, two-way ANOVA with repeated measures followed by Bonferroni post-hoc test). (**H** to **L**) Animals underwent the same protocol as in (A) to (E), except the virus injection was targeted to CA1. Representative images of CA1 from these animals are shown in (H) to (K), and the quantifications are shown in (L) (n = 4 subjects each; *P = 0.009, unpaired Student's t test). (**M**) Same as (F), except the viral injection and implants were targeted to CA1 (n = 8 subjects for ChR2-mCherry and mCherry groups; n.s., not significant; two-way ANOVA with repeated measures followed by Bonferroni post-hoc test). (**N**) Same as (G), except the viral injection and implants were targeted to CA1 (n = 6 subjects for ChR2-mCherry group and n = 5 subjects for mCherry group). Scale bar in (A) and (H), 250 μm.

whether this applies to a false fear memory, we examined fear-memory recall of experimental and control groups of mice in a distinct context (context D) with light-off and light-on epochs (Fig. 3B). All groups exhibited background levels of freezing during light-off epochs. The experimental group, however, froze at significantly higher levels (~25%) during light-on epochs. This light-induced freezing in context D was not observed in control animals that underwent the same behavioral schedule but did not receive light during fear conditioning in context B, in animals expressing mCherry alone, in animals receiving immediate shock, or in animals in which CA1 was manipulated instead (Fig. 3B and figs. S2D, S3C, S4C, and S5B).

Moreover, we quantified the levels of c-Fos expression in the basolateral amygdala (BLA) and the central amygdala (CeA) during the recall of a false and genuine fear memory (*15*–*20*). Both sessions elicited a significant increase in c-Fos–positive cells in the BLA and CeA compared with a control group exploring a neutral context (Fig. 3, C to F).

Last, a new cohort of mice was trained in a conditioned place avoidance (CPA) paradigm (*21*). Naïve animals did not show an innate preference for either chamber across multiple days (fig. S6A). An experimental group injected with the ChR2-mCherry virus and a control group injected with the mCherry-only virus were taken off Dox and exposed to one chamber of the CPA apparatus in order to label the DG cells activated in this chamber. These animals were then placed back on Dox and on the following day were exposed to the opposite chamber. Next, the mice were fear conditioned in a different context with light stimulation. The following day, they were placed back into the CPA apparatus, and their preference between the chambers was measured (Fig. 4A). After conditioning, the experimental group showed a strong preference for the unlabeled chamber over the labeled chamber, whereas the mCherry-only group spent an equal amount of time exploring both chambers (Fig. 4, B to D, and fig. S6B). Exposure to the two chambers activated a statistically independent population of DG cells (Fig. 4, E to K). We conducted similar behavioral tests targeting the CA1 subregion of the hippocampus, and the experimental group did not show any chamber preference (Fig. 4, L and M).

Our results show that cells activated previously in the hippocampal DG region can subsequently serve as a functional CS in a fear-conditioning paradigm when artificially reactivated during the delivery of a unconditioned stimulus (US). The consequence is the formation of a false associative fear memory to the CS that was not naturally available at the time of the US delivery. This is consistent with previous findings that high-frequency stimulation of the perforant path, an input to DG, can serve as a CS in a conditioned suppression paradigm (*22*).

Memory is constructive in nature; the act of recalling a memory renders it labile and highly

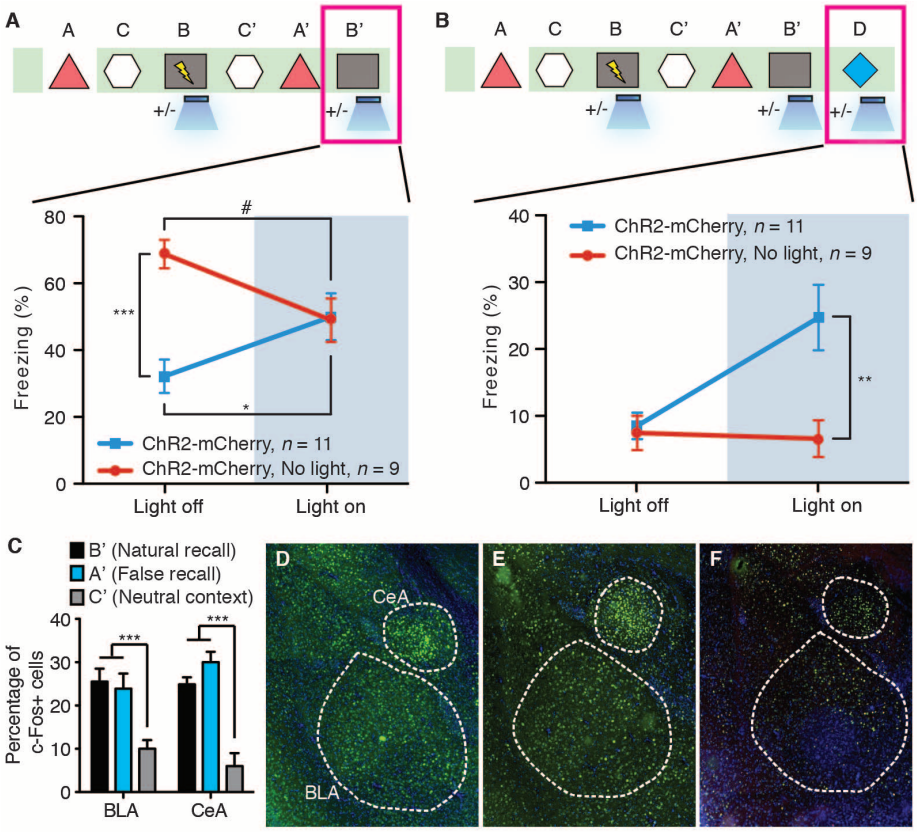

Fig. 3. The false and genuine fear memories interact with each other, and both recruit the amygdala. (**A**) Animals that underwent the behavioral protocol shown in Fig. 2G were reexposed to context B, and the freezing levels were examined both in the absence and presence of light stimulation (n = 11 subjects for ChR2-mCherry group and n = 9 subjects for ChR2-mCherry, no-light group; *P = 0.027; ***P < 0.001; #P = 0.034, two-way ANOVA with repeated measures followed by Bonferroni post-hoc test). (**B**) Animals that underwent the behavioral protocol shown in (A) were placed in a novel context D, and the freezing levels were examined both in the absence and presence of light stimulation (n = 11 subjects for ChR2-mCherry group and n = 9 subjects for ChR2-mCherry, no-light group; **P = 0.007, two-way ANOVA with repeated measures followed by Bonferroni post-hoc test). (**C**) Three groups of mice underwent the training shown in (A) and were euthanized after testing in either context B (natural recall), A (false recall), or C (neutral context). The percentage of c-Fos–positive cells was calculated for each group in basolateral amygdala (BLA) and central amygdala (CeA) (n = 6 subjects each; ***P < 0.001). (**D** to **F**) Images for natural recall, false recall, or neutral context.

susceptible to modification (*23*, *24*). In humans, memory distortions and illusions occur frequently. These phenomena often result from the incorporation of misinformation into memory from external sources (*25*–*27*). Cognitive studies in humans have reported robust activity in the hippocampus during the recall of both false and genuine memories (*28*). However, human studies performed using behavioral and functional magnetic resonance imaging techniques have not been able to delineate the hippocampal subregions and circuits that are responsible for the generated false memories. Our experiments provide an animal model in which false and genuine memories can be investigated at the memory-engram level (*29*). We propose that optical reactivation of cells that were naturally activated during the formation of a contextual memory induced the retrieval of that memory, and the retrieved memory became associated with an event of high valence (a foot shock) to form a new but false memory. Thus, the experimental group of animals showed increased freezing in a context in which they were never shocked (context A). Although our design for the formation and expression of a false memory was for a laboratory setting, and the retrieval of the contextual memory during conditioning occurred by artificial means (light), we speculate that the formation of at least some false memories in humans may occur in natural settings through the internally driven retrieval of a previously formed memory and its association with concurrent external stimuli of high valence.

Our experiments also allowed us to examine the dynamic interaction between the false and genuine memories at different stages of the memory process. During the acquisition phase, the artificial contextual information (context A by light activation) either competed with the genuine contextual cues (context B by natural exposure) for the valence of the US (foot shock), or may have interfered with the perception of the genuine

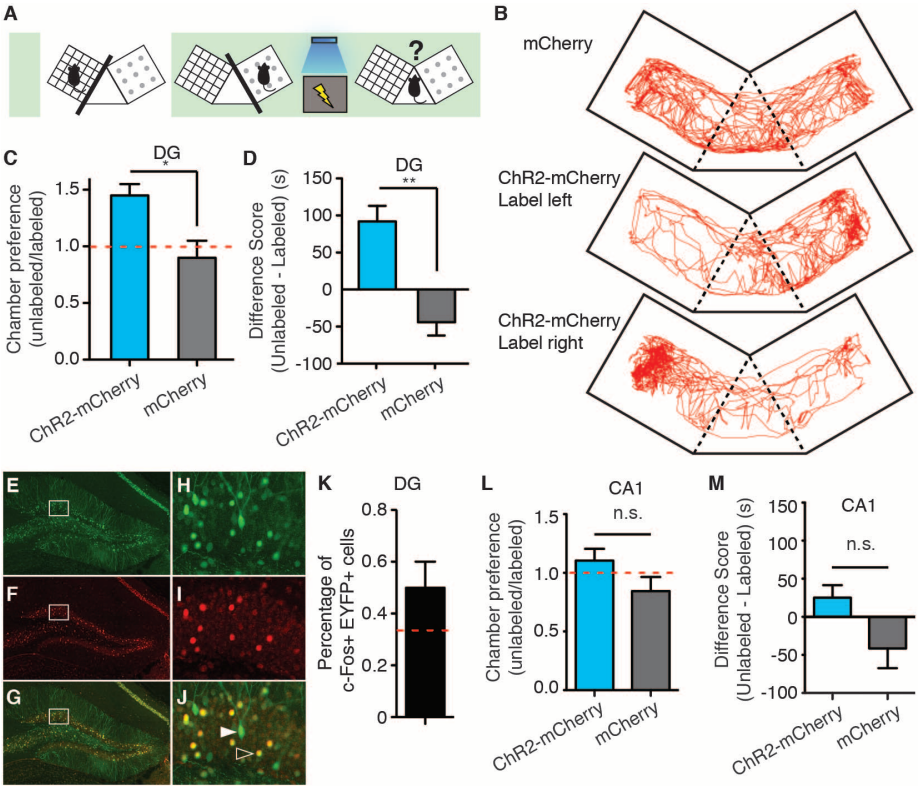

Fig. 4. The false memory supports active fear behavior. (**A**) The scheme for conditioned place-avoidance paradigm. Various symbols are as explained in Fig. 1. (**B**) Locomotion traces during testing from animals injected with AAV_9-TRE-mCherry (top), or animals injected with AAV_9-TRE-ChR2-mCherry and DG cells subsequently labeled, corresponding to either the left (middle) or right (bottom) chamber. (**C** and **D**) ChR2-mCherry and mCherry group preferences for the labeled versus unlabeled chambers as shown by the ratio (C) or the difference in duration of the time spent in each chamber (D). ($n = 8$ subjects; $^*P = 0.013$; $^{**}P = 0.008$, unpaired Student's t test). The red dashed line indicates no preference. (**E** to **K**), c-fos-tTA mice injected with AAV_9-TRE-EYFP in the DG were taken off Dox and exposed to one chamber in order to label the activated cells with EYFP (green) then put back on Dox and exposed to the opposite chamber 24 hours later to let activated cells express c-Fos (red). Expression of EYFP [(E) and (H)], expression of c-Fos [(F) and (I)], and a merged view [(G) and (J)] are shown. Solid arrows indicate cells expressing EYFP. Open arrows indicate cells expressing c-Fos. These cells appear yellow because they express both endogenous c-Fos (red) and the nuclear-localized c-fos-shEGFP (green) from the mouse line (*10*). Quantifications from the dorsal blades of the DG are shown in (K) ($n = 4$ subjects). Red dashed lines indicate the chance level of overlap. (**L** and **M**) Same as (C) and (D), except the viral injection and implants were targeted to CA1 ($n = 6$ subjects each group).

contextual cues. This resulted in reduced expression of both false and genuine fear memories compared with the strength of recall attainable after normal fear conditioning (Fig. 3A, the two groups during the light-off epoch). This could also be related to the overshadowing effects for multiple CSs (*30*). During the recall phase in context B, the false memory and the genuine memory were either additive (Fig. 3A, the with-light group during light-off and light-on epochs) or competitive (Fig. 3A, the no light group during light-off and light-on epochs). All of these observations are consistent with the predictions of an updated Rescorla-Wagner componential model for two independent CSs and suggest that the light-activated artificial CS is qualitatively similar to the genuine CS (*14*).

A previous study applied a similar experimental protocol with pharmacosynthetic methods and failed to see increased freezing upon reexposure to either context A or context B. Instead, they observed a synthetic memory that could only be retrieved by the combination of both contexts A and B (*9*). A key difference in their system is that the c-Fos–expressing cells in the entire forebrain were labeled and reactivated over an extended period by a synthetic ligand. We propose that activating neurons in much wider spatial and temporal domains may favor the formation of a synthetic memory, which may not be easily retrievable by the cues associated with each individual memory. In contrast, activating neurons in a more spatially (only small populations of DG cells) and temporally restricted manner (only a few minutes during light stimulation) may favor the formation of two distinct (false and genuine) memories as observed in our case. In line with this hypothesis, when we manipulated CA1 cells by the same procedures as the ones used for DG cells, we could not create a false memory (freezing in context A). In CA1, the overlap of the cell populations activated by consecutive exposures to a pair of contexts is much greater than in the DG. Although additional work is needed to reveal the nature of CA1 engrams, we hypothesize that our negative CA1 behavioral data could be a result of contextual engrams relying less on a population code and increasingly on a temporal code as they travel through the trisynaptic circuit (*4*, *11*–*13*).

References and Notes

1. D. L. Schacter, D. R. Addis, R. L. Buckner, *Nat. Rev. Neurosci.* **8**, 657–661 (2007).
2. E. Pastalkova, V. Itskov, A. Amarasingham, G. Buzsáki, *Science* **321**, 1322–1327 (2008).
3. H. Gelbard-Sagiv, R. Mukamel, M. Harel, R. Malach, I. Fried, *Science* **322**, 96–101 (2008).
4. C. J. MacDonald, K. Q. Lepage, U. T. Eden, H. Eichenbaum, *Neuron* **71**, 737–749 (2011).
5. G. Buzsáki, E. I. Moser, *Nat. Neurosci.* **16**, 130–138 (2013).
6. T. J. McHugh *et al.*, *Science* **317**, 94–99 (2007).
7. D. Tse *et al.*, *Science* **316**, 76–82 (2007).
8. X. Liu *et al.*, *Nature* **484**, 381–385 (2012).
9. A. R. Garner *et al.*, *Science* **335**, 1513–1516 (2012).
10. L. G. Reijmers, B. L. Perkins, N. Matsuo, M. Mayford, *Science* **317**, 1230–1233 (2007).
11. S. Kubik, T. Miyashita, J. F. Guzowski, *Learn. Mem.* **14**, 758–770 (2007).
12. J. F. Guzowski, B. L. McNaughton, C. A. Barnes, P. F. Worley, *Nat. Neurosci.* **2**, 1120–1124 (1999).
13. J. K. Leutgeb, S. Leutgeb, M. B. Moser, E. I. Moser, *Science* **315**, 961–966 (2007).
14. S. E. Brandon, E. H. Vogel, A. R. Wagner, *Behav. Brain Res.* **110**, 67–72 (2000).
15. J. H. Han *et al.*, *Science* **323**, 1492–1496 (2009).
16. M. T. Rogan, U. V. Stäubli, J. E. LeDoux, *Nature* **390**, 604–607 (1997).
17. J. P. Johansen *et al.*, *Proc. Natl. Acad. Sci. U.S.A.* **107**, 12692–12697 (2010).
18. S. Maren, G. J. Quirk, *Nat. Rev. Neurosci.* **5**, 844–852 (2004).
19. H. Li *et al.*, *Nat. Neurosci.* **16**, 332–339 (2013).
20. S. Ciocchi *et al.*, *Nature* **468**, 277–282 (2010).
21. S. Lammel *et al.*, *Nature* **491**, 212–217 (2012).
22. V. Doyère, S. Laroche, *Hippocampus* **2**, 39–48 (1992).
23. K. Nader, G. E. Schafe, J. E. Le Doux, *Nature* **406**, 722–726 (2000).
24. F. C. Bartlett, *Remembering: A Study in Experimental and Social Psychology* (Cambridge Univ. Press, Cambridge, 1932).
25. E. F. Loftus, *Nat. Rev. Neurosci.* **4**, 231–234 (2003).
26. D. L. Schacter, E. F. Loftus, *Nat. Neurosci.* **16**, 119–123 (2013).
27. H. L. Roediger, K. B. McDermott, *J. Exp. Psychol. Learn. Mem. Cogn.* **24**, 803–814 (1995).
28. R. Cabeza, S. M. Rao, A. D. Wagner, A. R. Mayer, D. L. Schacter, *Proc. Natl. Acad. Sci. U.S.A.* **98**, 4805–4810 (2001).
29. S. M. McTighe, R. A. Cowell, B. D. Winters, T. J. Bussey, L. M. Saksida, *Science* **330**, 1408–1410 (2010).
30. I. P. Pavlov, *Conditioned Reflexes* (Oxford University Press, Oxford, 1927).

Acknowledgments: We thank S. Huang, M. Serock, A. Mockett, J. Zhou, and D. S. Roy for help with the experiments; J. Z. Young and K. L. Mulroy for comments and discussions on the manuscript; and all the members of the Tonegawa lab for their support. This work was supported by the RIKEN Brain Science Institute.

Supplementary Materials

www.sciencemag.org/cgi/content/full/341/6144/387/DC1
Materials and Methods
Figs. S1 to S6
References

12 April 2013; accepted 2 July 2013
10.1126/science.1239073

Cell Stem Cell
Article

Highly Efficient Reprogramming to Pluripotency and Directed Differentiation of Human Cells with Synthetic Modified mRNA

Luigi Warren,[1,17] Philip D. Manos,[2,4,17] Tim Ahfeldt,[4,6,7,18] Yuin-Han Loh,[8,9,18] Hu Li,[11,12,18] Frank Lau,[4,13] Wataru Ebina,[1] Pankaj K. Mandal,[1] Zachary D. Smith,[14] Alexander Meissner,[4,5,14] George Q. Daley,[2,3,4,5,8,15,16] Andrew S. Brack,[5,6] James J. Collins,[11,12,15] Chad Cowan,[4,5,6,13] Thorsten M. Schlaeger,[2,8] and Derrick J. Rossi[1,2,5,10,*]

[1]Immune Disease Institute, Program in Cellular and Molecular Medicine
[2]Stem Cell Program
[3]Manton Center for Orphan Disease Research
Children's Hospital Boston, Boston, MA 02115, USA
[4]Department of Stem Cell and Regenerative Biology
[5]Harvard Stem Cell Institute
Harvard University, Cambridge, MA 02138, USA
[6]Center of Regenerative Medicine, Massachusetts General Hospital, 185 Cambridge Street, Boston, MA 02114-2790, USA
[7]Department of Biochemistry and Molecular Biology II: Molecular Cell Biology, University Medical Center Hamburg-Eppendorf, Hamburg 20246, Germany
[8]Division of Pediatric Hematology/Oncology, Children's Hospital Boston and Dana-Farber Cancer Institute, Boston, MA 02115, USA
[9]Department of Biological Chemistry and Molecular Pharmacology
[10]Department of Pathology
Harvard Medical School, Boston, MA 02115, USA
[11]Department of Biomedical Engineering and Center for BioDynamics, Boston University, Boston, MA 02215, USA
[12]Wyss Institute for Biologically Inspired Engineering, Harvard University, Boston, MA 02115, USA
[13]Stowers Medical Institute, 185 Cambridge Street, Boston, MA 02114, USA
[14]Broad Institute of MIT and Harvard, Cambridge, MA 02142, USA
[15]Howard Hughes Medical Institute
[16]Division of Hematology/Oncology, Brigham and Women's Hospital, Boston, MA 02115, USA
[17]These authors contributed equally to this work
[18]These authors contributed equally to this work
*Correspondence: rossi@idi.harvard.edu
DOI 10.1016/j.stem.2010.08.012

SUMMARY

Clinical application of induced pluripotent stem cells (iPSCs) is limited by the low efficiency of iPSC derivation and the fact that most protocols modify the genome to effect cellular reprogramming. Moreover, safe and effective means of directing the fate of patient-specific iPSCs toward clinically useful cell types are lacking. Here we describe a simple, nonintegrating strategy for reprogramming cell fate based on administration of synthetic mRNA modified to overcome innate antiviral responses. We show that this approach can reprogram multiple human cell types to pluripotency with efficiencies that greatly surpass established protocols. We further show that the same technology can be used to efficiently direct the differentiation of RNA-induced pluripotent stem cells (RiPSCs) into terminally differentiated myogenic cells. This technology represents a safe, efficient strategy for somatic cell reprogramming and directing cell fate that has broad applicability for basic research, disease modeling, and regenerative medicine.

INTRODUCTION

The reprogramming of differentiated cells to pluripotency holds great promise as a tool for studying normal development, while offering hope that patient-specific induced pluripotent stem cells (iPSCs) could be used to model disease or to generate clinically useful cell types for autologous therapies aimed at repairing deficits arising from injury, illness, and aging. Induction of pluripotency was originally achieved by Yamanaka and colleagues by enforced expression of four transcription factors, KLF4, c-MYC, OCT4, and SOX2 (KMOS), by using retroviral vectors (Takahashi et al., 2007; Takahashi and Yamanaka, 2006). Viral integration into the genome initially presented a formidable obstacle to therapeutic use of iPSCs. The search for ways to induce pluripotency without incurring genetic change has thus become the focus of intense research effort. Toward this end, iPSCs have been derived via excisable lentiviral and transposon vectors or through repeated application of transient plasmid, episomal, and adenovirus vectors (Chang et al., 2009; Kaji et al., 2009; Okita et al., 2008; Stadtfeld et al., 2008; Woltjen et al., 2009; Yu et al., 2009). iPSCs have also been derived with two DNA-free methods: serial protein transduction with recombinant proteins incorporating cell-penetrating peptide moieties (Kim et al., 2009; Zhou et al., 2009) and transgene

delivery using the Sendai virus, which has a completely RNA-based reproductive cycle (Fusaki et al., 2009).

Despite such progress, considerable limitations accompany the nonintegrative iPSC derivation strategies devised thus far. For example, although DNA transfection-based methodologies are ostensibly safe, they nonetheless entail some risk of genomic recombination or insertional mutagenesis. In protein-based strategies, the recombinant proteins used are challenging to generate and purify in the quantities required (Zhou et al., 2009). Use of Sendai virus requires stringent steps to purge reprogrammed cells of replicating virus, and the sensitivity of the viral RNA replicase to transgene sequence content may limit the generality of this reprogramming vehicle (Fusaki et al., 2009). Importantly, methods that rely on repeat administration of transient vectors, whether DNA or protein based, have so far shown very low iPSC derivation efficiencies (Jia et al., 2010; Kim et al., 2009; Okita et al., 2008; Stadtfeld et al., 2008; Yu et al., 2009; Zhou et al., 2009), presumably because of weak or inconstant expression of reprogramming factors.

Here we demonstrate that repeated administration of synthetic messenger RNAs incorporating modifications designed to bypass innate antiviral responses can reprogram differentiated human cells to pluripotency with conversion efficiencies and kinetics substantially superior to established viral protocols. Furthermore, this simple, nonmutagenic, and highly controllable technology is applicable to a range of tissue-engineering tasks, exemplified here by RNA-mediated directed differentiation of RNA-iPSCs (RiPSCs) to terminally differentiated myogenic cells.

RESULTS

Development of Modified RNAs for Directing Cell Fate

We manufactured mRNA by using in vitro transcription (IVT) reactions templated by PCR amplicons (Figure S1 available online). To promote efficient translation and boost RNA half-life in the cytoplasm, a 5′ guanine cap was incorporated by inclusion of a synthetic cap analog in the IVT reactions (Yisraeli and Melton, 1989). Within our IVT templates, the open reading frame (ORF) of the gene of interest is flanked by a 5′ untranslated region (UTR) containing a strong Kozak translational initiation signal and an alpha-globin 3′ UTR terminating with an oligo(dT) sequence for templated addition of a polyA tail.

Cytosolic delivery of mRNA into mammalian cells can be achieved via electroporation or by complexing the RNA with a cationic vehicle to facilitate uptake by endocytosis (Audouy and Hoekstra, 2001; Elango et al., 2005; Holtkamp et al., 2006; Van den Bosch et al., 2006; Van Tendeloo et al., 2001). We focused on the latter approach, reasoning that this would allow for repeated transfection to sustain ectopic protein expression over the days to weeks required for cellular reprogramming. In preliminary experiments in which synthetic RNA encoding GFP was transfected into murine embryonic fibroblasts and human epidermal keratinocytes, a high, dose-dependent cytotoxicity was observed that was not attributable to the cationic vehicle, which was exacerbated on repeated transfection. These experiments revealed a serious impediment to achieving sustained protein expression by mRNA transfection and highlighted a need to develop a technology that would permit sustained protein expression with mRNA with reduced cellular toxicity.

It is known that exogenous single-stranded RNA (ssRNA) activates antiviral defenses in mammalian cells through interferon- and NF-κB-dependent pathways (Diebold et al., 2004; Hornung et al., 2006; Kawai and Akira, 2007; Pichlmair et al., 2006; Uematsu and Akira, 2007). We sought approaches to reduce the immunogenic profile of synthetic RNA in order to increase the sustainability of RNA-mediated protein expression. Cotranscriptional capping yields a significant fraction of uncapped IVT products bearing 5′ triphosphates, which can be detected by the ssRNA sensor RIG-I (Hornung et al., 2006; Pichlmair et al., 2006), and have also been reported to activate PKR, a global repressor of protein translation (Nallagatla and Bevilacqua, 2008). We therefore treated synthesized RNA with a phosphatase, which resulted in modest reductions in cytotoxicity upon transfection (data not shown).

Eukaryotic mRNA is extensively modified in vivo, and the presence of modified nucleobases has been shown to reduce signaling by RIG-I and PKR, as well as by the less widely expressed but inducible endosomal ssRNA sensors TLR7 and TLR8 (Karikó et al., 2005, 2008; Karikó and Weissman, 2007; Nallagatla and Bevilacqua, 2008; Nallagatla et al., 2008; Uzri and Gehrke, 2009). In an attempt to further reduce innate immune responses to transfected RNA, we synthesized mRNAs incorporating modified ribonucleoside bases. Complete substitution of either 5-methylcytidine (5mC) for cytidine or pseudouridine (psi) for uridine in GFP-encoding transcripts markedly improved viability and increased ectopic protein expression, although the most significant improvement was seen when both modifications were used together (Figures 1A–1C). These modifications dramatically attenuated interferon signaling as revealed by qRT-PCR for a panel of interferon response genes, although residual upregulation of some interferon targets was still detected (Figure 1D). It is known that cellular antiviral defenses can self-prime through a positive-feedback loop involving autocrine and paracrine signaling by type I interferons (Randall and Goodbourn, 2008). Media supplementation with a recombinant version of B18R protein, a Vaccinia virus decoy receptor for type I interferons (Symons et al., 1995), further increased cell viability of RNA transfection in some cell types (data not shown). Synthesis of RNA with modified ribonucleotides and phosphatase treatment (henceforth, modified RNAs), used in conjunction with media supplementation with the interferon inhibitor B18R, allowed for high, dose-dependent levels of protein expression with high cell viability (Figure 1E).

Transfection of modified RNA encoding GFP into six human cell types showed highly penetrant expression (50%–90% positive cells), demonstrating the applicability of this technology to diverse cell types (Figure S2A). Simultaneous delivery of modified RNAs encoding mCherry and GFP containing a nuclear localization signal confirmed that generalized coexpression of multiple proteins could be achieved in mammalian cells and that expressed proteins could be correctly localized to different cellular compartments (Figure 1F). Ectopic protein expression after RNA transfection is transient owing to RNA and protein degradation and the diluting effect of cell division. To establish the kinetics and persistence of protein expression, modified RNA encoding GFP variants designed for high and low protein stability (Li et al., 1998) were synthesized and transfected into keratinocytes. Time course analysis by flow cytometry showed

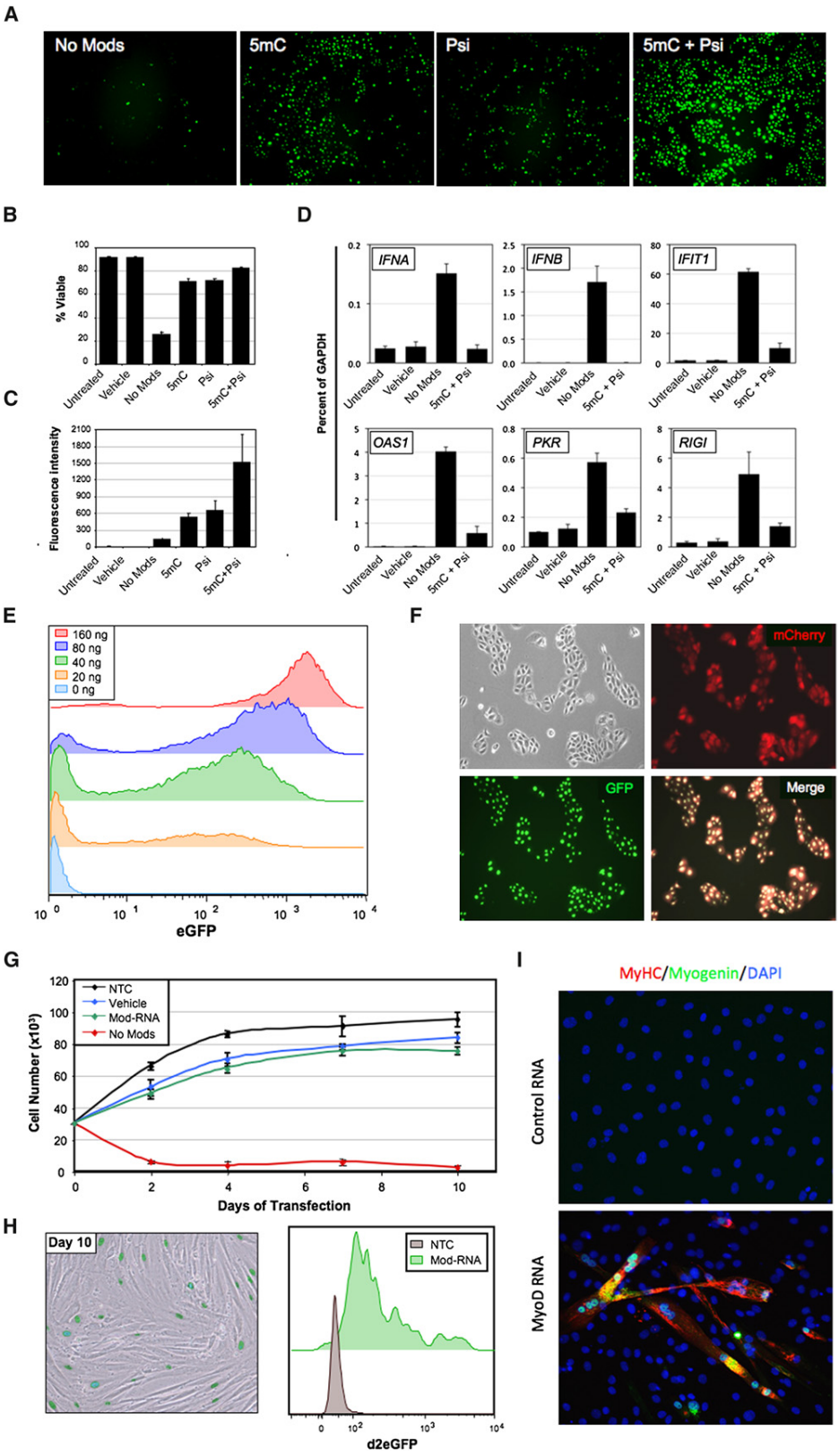
A
No Mods
5mC
Psi
5mC + Psi
B
% Viable
Untreated
Vehicle
No Mods
5mC
Psi
5mC+Psi
C
Fluorescence Intensity
D
Percent of GAPDH
IFNA
IFNB
IFIT1
OAS1
PKR
RIGI
E
160 ng
80 ng
40 ng
20 ng
0 ng
eGFP
F
mCherry
GFP
Merge
G
NTC
Vehicle
Mod-RNA
No Mods
Cell Number (x10³)
Days of Transfection
H
Day 10
NTC
Mod-RNA
d2eGFP
I
MyHC/Myogenin/DAPI
Control RNA
MyoD RNA

that protein expression persisted for several days for the high-stability variant but peaked within 12 hr and decayed rapidly thereafter for the destabilized GFP (Figure S2B). These results indicated that a repetitive transfection regimen would be required to sustain high levels of ectopic expression for short-lived proteins over an extended time course. To address this and further examine the impact of repeated RNA transfection on cell growth and viability, we transfected BJ fibroblasts for 10 consecutive days with either unmodified or modified RNAs encoding a destabilized nuclear GFP and appropriate controls (Figure S3A). Daily transfection with modified RNA permitted sustained protein expression without substantially compromising the viability of the culture beyond a modest reduction in growth kinetics that was largely attributable to the transfection reagent (Figures 1G and 1H; Figure S2C). Microarray analysis of the cultures after the tenth and final transfection revealed that prolonged daily transfection with modified RNA did not significantly alter the molecular profile of the transfected cells (Figure S2D), although upregulation of a number of interferon response genes was noted, consistent with our previous observation that the RNA modifications did not completely abrogate interferon signaling (Figure 1D; Figure S2E). By contrast, repeated transfection with unmodified RNA severely compromised the growth and viability of the culture through elicitation of a massive interferon response (Figure 1D), indicating that the use of unmodified RNA was not a viable strategy for sustaining polypeptide expression in cells (Figure 1G).

To determine whether modified RNAs could be used to directly alter cell fate, we synthesized modified RNA encoding the myogenic transcription factor *MYOD* (Davis et al., 1987) and transfected it into murine C3H10T1/2 cells over the course of 3 days, followed by continued culturing in a low serum media for an additional 3 days. The emergence of large, multinucleated myotubes that stained positive for the myogenic markers myogenin and myosin heavy chain (MyHC) provided proof of principle that transfection with modified RNAs could be utilized to efficiently direct cell fate (Figure 1I).

Generation of Induced Pluripotent Stem Cells via Modified RNAs

We next sought to determine whether induced pluripotent stem cells (iPSCs) could be derived via modified RNAs. To this end, modified RNAs encoding the four canonical Yamanaka factors, *KLF4* (K), *c-MYC* (M), *OCT4* (O), and *SOX2* (S), were synthesized and transfected into cells. Immunostaining with antibodies directed against OCT4, KLF4, and SOX2 demonstrated that each of the factors was robustly expressed and correctly localized to the nucleus (Figure 2A). Expression kinetics was monitored by flow cytometry, which showed maximal protein expression 12 to 18 hours after transfection, followed by rapid turnover of these transcription factors (Figure 2B). From this we concluded that daily transfections would be required to maintain high levels of expression of the Yamanaka factors during long-term, multifactor reprogramming regimens.

We next sought to establish a protocol to ensure sustained, high-level protein expression through daily transfection of modified RNAs by exploring a matrix of conditions encompassing different transfection reagents, culture media, feeder cell types, and RNA doses (data not shown). Once optimized, we initiated long-term reprogramming experiments with human ESC-derived dH1f fibroblasts, which display relatively efficient viral-mediated iPSC conversion (Chan et al., 2009; Park et al., 2008). Low-oxygen (5% O_2) culture conditions and a KMOS stoichiometry of 1:1:3:1 were employed, because these have been reported to promote efficient iPSC conversion (Kawamura et al., 2009; Papapetrou et al., 2009; Utikal et al., 2009; Yoshida et al., 2009). Modified RNA encoding a destabilized nuclear GFP was spiked into the KMOS RNA cocktail to allow visualization of continued protein expression throughout the experimental time course (Figure S3A). Widespread transformation of fibroblast morphology to a compact, epithelioid morphology was observed within the first week of modified RNA transfection, followed by emergence of canonical hESC-like colonies with tight morphology, well-defined borders, and prominent nucleoli toward the end of the second week of transfection (Figure 2C). RNA transfection was terminated on day 17, and colonies were mechanically picked 3 days later, which were then expanded under standard ESC culture conditions to establish 14 prospective iPSC lines, designated dH1f-RiPSC (RNA-derived iPSC) 1–14.

We next attempted to reprogram somatically derived cells to pluripotency by using a similar reprogramming regimen. Anticipating that these cells might be more challenging to reprogram, we employed a five-factor cocktail including a modified RNA encoding LIN28 (KMOSL), which has been shown to facilitate reprogramming (Yu et al., 2007; Hanna et al., 2009), and we supplemented the media with valproic acid (VPA), a histone deacetylase inhibitor that has been reported to increase reprogramming efficiency (Huangfu et al., 2008). Four human cell types were tested: Detroit 551 (D551) and MRC-5 fetal fibroblasts, BJ

Figure 1. Modified RNA Overcomes Antiviral Responses and Can Be Used to Direct Cell Fate

(A) Microscopy images showing keratinocytes transfected 24 hr earlier with 400 ng/well of synthetic unmodified (No Mods), 5-methyl-cytosine modified (5mC), pseudouridine modified (Psi), or 5mC + Psi modified RNA encoding GFP.

(B and C) Percent viability (B) and mean fluorescence intensity (C) of the cells shown in (A) as measured by flow cytometry.

(D) Quantitative RT-PCR data showing expression of six interferon-regulated genes in BJ fibroblasts 24 hr after transfection with unmodified (No Mods) or modified (5mC + Psi) RNA encoding GFP (1200 ng/well), and vehicle and untransfected controls.

(E) Flow cytometry histograms showing GFP expression in keratinocytes transfected with 0–160 ng of modified-RNA, 24 hr posttransfection.

(F) Microscopy images of keratinocytes cotransfected with modified RNAs encoding GFP with a nuclear localization signal, and mCherry (cytosolic) proteins.

(G) Growth kinetics of BJ fibroblasts transfected daily with unmodified or modified RNAs encoding a destabilized nuclear-localized GFP, and vehicle and untransfected controls for 10 days.

(H) Sustained GFP expression of modified RNA-transfected cells described in (G) at day 10 of transfection shown by fluorescence imaging with bright field overlay (left) and flow cytometry (right).

(I) Immunostaining for the muscle-specific proteins myogenin and myosin heavy chain (MyHC) in murine C3H/10T1/2 cell cultures 3 days after three consecutive daily transfections with a modified RNA encoding *MYOD*.

Error bars indicate SD, n = 3 for all panels. See also Figure S2.

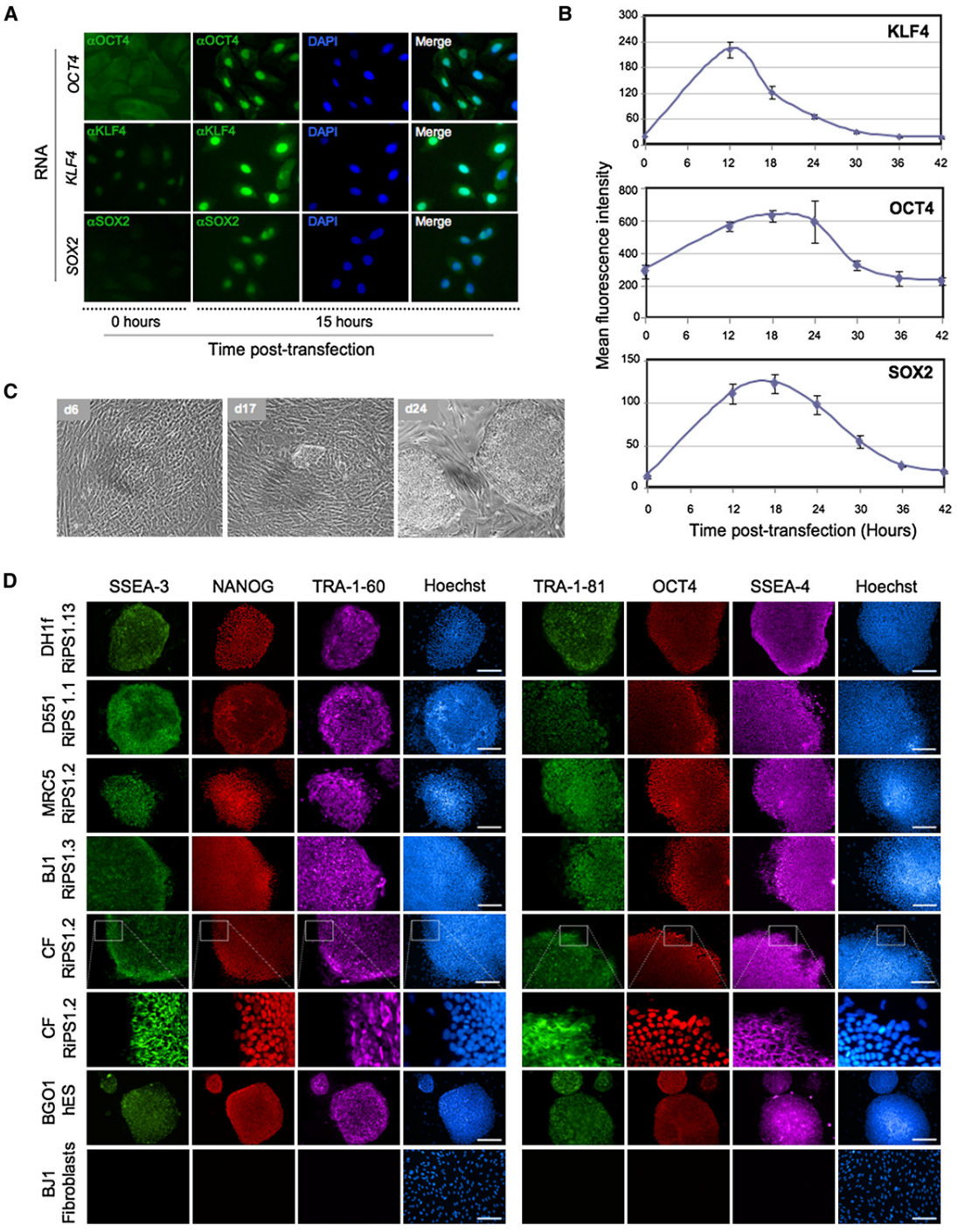

Figure 2. Generation of RNA-Induced Pluripotent Stem Cells

(A) Immunostaining for human KLF4, OCT4, and SOX2 proteins in keratinocytes 15 hr posttransfection with modified RNA encoding KLF4, OCT4, or SOX2.

(B) Time course showing kinetics and stability of KLF4, OCT4, and SOX2 proteins after modified RNA transfection, assayed by flow cytometry after intracellular staining of each protein.

(C) Bright-field images taken during the derivation of RNA-iPSCs (RiPS) from dH1f fibroblasts showing early epitheliod morphology (day 6), small hESC-like colonies (day 17), and appearance of mature iPSC clones after mechanical picking and expansion (day 24).

(D) Immunohistochemistry showing expression of a panel of pluripotency markers in expanded RiPSC clones derived from dH1f fibroblasts, Detroit 551 (D551) and MRC-5 fetal fibroblasts, BJ postnatal fibroblasts, and cells derived from a skin biopsy taken from an adult cystic fibrosis patient (CF), shown also in high magnification. BG01 hESCs and BJ1 fibroblasts are included as positive and negative controls, respectively. Scale bars represent 200 μm.

See also Figures S3 and S4.

postnatal fibroblasts, and fibroblast-like cells cultured from a primary skin biopsy taken from an adult cystic fibrosis patient (CF cells). Daily transfection with the modified RNA KMOSL cocktail gave rise to numerous hESC-like colonies in the D551, BJ, CF, and MRC5 cultures that were mechanically picked at day 18, 20, 21, and 25, respectively. More than 10 RiPSC clones were expanded for each of the somatic lines, with notably very few clones failing to establish. Immunostaining confirmed the expression of OCT4, NANOG, TRA-1-60, TRA-1-81, SSEA3, and SSEA4 in all the RiPSC lines examined (Figure 2D; Figure S3B). DNA fingerprinting confirmed parental origin of three RiPSC clones from each somatic cell derivation, and all clones presented normal karyotypes (data not shown). Of note, additional experiments conducted in the presence or absence of VPA showed little difference in reprogramming efficiency (data not shown), and VPA was therefore not used in subsequent experiments.

Molecular Characterization and Functional Potential of RiPSCs

A number of molecular and functional assays were performed to further assess whether the RiPSCs had been reprogrammed to pluripotency (Table S1). Multiple RiPSC lines derived from each of the five starting cell types were evaluated by quantitative RT-PCR (qRT-PCR), and all demonstrated robust expression of the pluripotency-associated transcripts *OCT4*, *SOX2*, *NANOG,* and *hTERT* (Figure 3A). Bisulfite sequencing of the Oct4 locus revealed extensive demethylation relative to the parental fibroblasts, an epigenetic state equivalent to human ESCs (Figure 3B).

To gain more global insight into the molecular properties of RiPSCs, gene expression profiles of RiPSC clones from multiple independent derivations were generated and compared to fibroblasts, human ESCs, and virally derived iPSC lines. These analyses revealed that all modified RNA-derived iPSC clones examined had a molecular signature that very closely recapitulated that of human ESCs while being highly divergent from the profile of the parental fibroblasts (Figure 3C). Importantly, pluripotency-associated transcripts including *SOX2, REX1, NANOG, OCT4, LIN28*, and *DNMT3B* were substantially upregulated in the RiPSCs compared to the parental fibroblast lines to levels comparable to hESCs (Figure 3C). Furthermore, when the transcriptional profiles were subjected to unsupervised hierarchical clustering analysis, all RiPSC clones analyzed clustered more closely to hESC than did virally derived iPSCs, suggesting that modified RNA-derived iPSCs more fully recapitulated the molecular signature of human ESCs (Figure 3D).

To test the developmental potential of RiPSCs, embryoid bodies (EBs) were generated from multiple clones from five independent RiPSC derivations, and beating cardiomyocytes were observed for the vast majority of the EBs (Table S1, Movie S1). Mesodermal potential was further evaluated in methylcellulose blood-forming assays that showed that all lines tested were robustly able to differentiate into hematopoietic precursors capable of giving rise to colony numbers and a spectrum of blood colony types comparable to human ESCs (Figure 4A; Table S1). A subset of clones was further plated onto matrigel and differentiated into Tuj1-positive neurons (ectoderm) and alpha-fetoprotein-positive endodermal cells (Figure 4B; Table S1). Finally, trilineage differentiation potential was confirmed in vivo by the formation of teratomas from dH1F-, CF-, and BJ-RiPSCs, which histologically revealed cell types of the three germ layers (Figure 4C; Figure S5, Table S1).

Taken together, these data demonstrate by the most stringent criteria available to human pluripotent cells (Chan et al., 2009; Smith et al., 2009) that modified RNA-derived iPSC clones from multiple independent derivations were reprogrammed to pluripotency and closely recapitulated the functional and molecular properties of human ESCs.

Modified RNAs Generate iPSCs at Very High Efficiency

During the course of our experiments, we noted surprisingly high reprogramming efficiencies and rapid kinetics with which RiPSCs were generated. To quantify this more thoroughly, a number of reprogramming experiments were undertaken in which quantitative readout of efficiency was based on colony morphology and expression of the stringent pluripotency markers TRA-1-60 and TRA-1-81 (Chan et al., 2009; Lowry et al., 2008). In one set of experiments, BJ fibroblasts transfected with a five-factor modified RNA cocktail (KMOSL) demonstrated an iPSC conversion efficiency of more than 2%, regardless of whether the cells were passaged in the presence or absence of Rho-associated kinase (ROCK), Y-27632 (Figures 5A and 5B; Table 1). This efficiency was two orders of magnitude higher than those typically reported for virus-based derivations. Moreover, in contrast to virus-mediated BJ-iPSC derivations, in which iPSC colonies typically take around 4 weeks to emerge, by day 17 of RNA transfection the plates had already become overgrown with ESC-like colonies (Figure 5A).

We next evaluated the contributions of low-oxygen culture and LIN28 to the efficiency of RiPSC derivation. The yield of TRA-1-60/TRA-1-81-positive colonies in the ambient (20%) oxygen condition was 4-fold lower than in the cultures maintained at 5% O_2 when using KMOS RNA, but this deficit was negated when LIN28 was added to the cocktail (Figures 5C and 5D; Table 1). The highest conversion efficiency (4.4%) was observed when low-oxygen culture and the five-factor KMOSL cocktail were combined.

To directly compare the kinetics and efficiency of our RiPSC derivation protocol against an established viral protocol, we conducted an experiment in which dH1f fibroblasts were transfected with either KMOS-modified RNAs or transduced with KMOS retroviruses in parallel. As had been observed in previous experiments, ESC-like colonies began to emerge toward the end of the second week on the RNA-transfected cultures, and the plates became overgrown with ESC-like colonies by the 16th and final day of transfection. By contrast, no ESC-like colonies had appeared in the retrovirally transduced cultures by this time point, and colonies began to emerge only on the 24th day post-transduction, a time point consistent with previous reports describing iPSC derivation by retroviruses (Lowry et al., 2008; Takahashi et al., 2007). The retroviral cultures were fixed for analysis on day 32. Both arms of the experiment were then immunostained for TRA-1-60 and colonies were counted. iPSC derivation efficiencies were 1.4% and 0.04% for modified RNA and retrovirus, respectively, corresponding to 36-fold higher conversion efficiency with the modified RNA protocol (Figures 5E and 5F; Table 1). These experiments also revealed that the

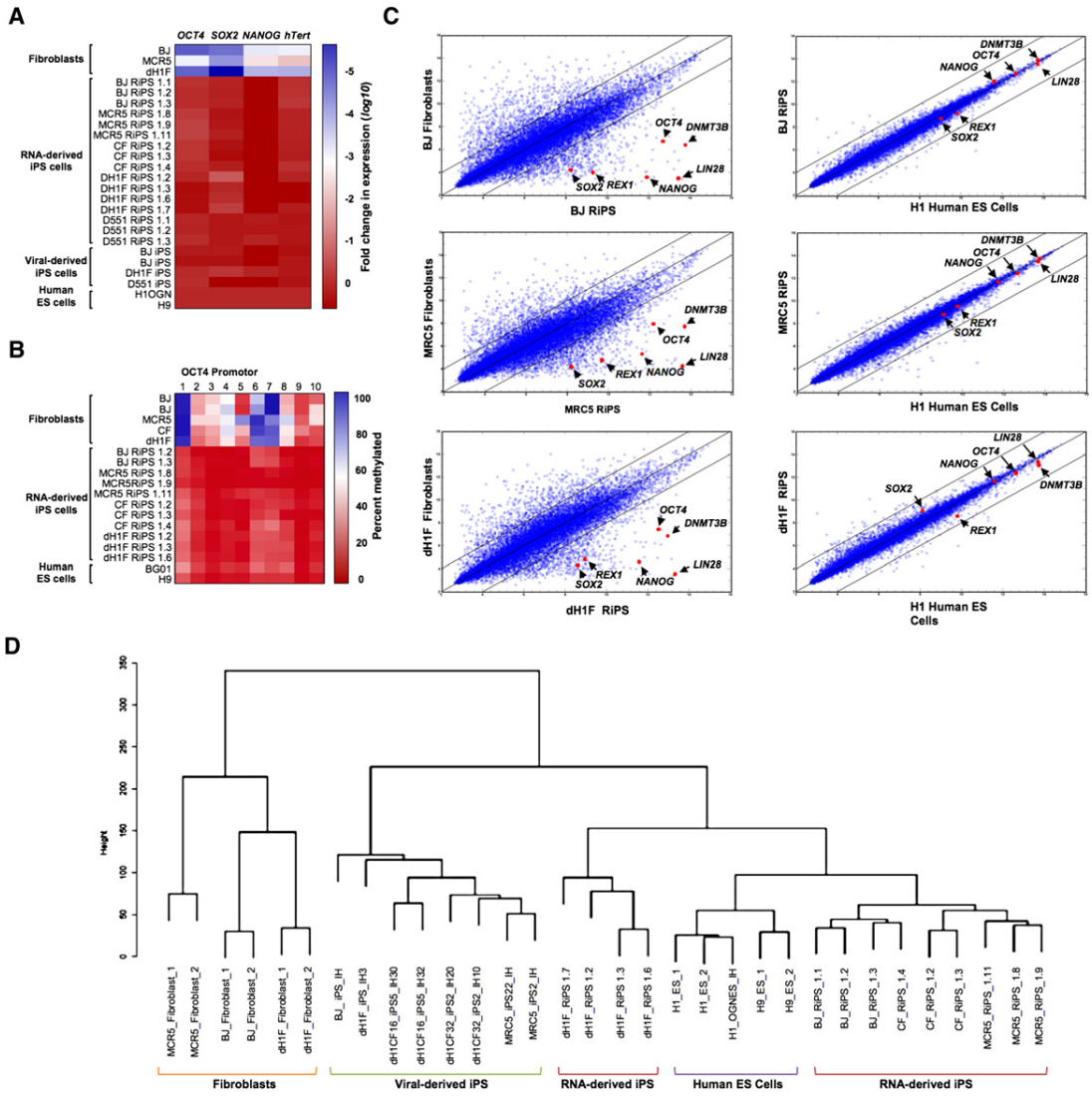

Figure 3. Molecular Characterization of RiPSCs

(A) Heatmap showing results of qRT-PCR analysis measuring the expression of pluripotency-associated genes in RiPSC lines, parental fibroblasts, and viral-derived iPSCs relative to hESC controls.

(B) Heatmap showing results of OCT4 promoter methylation analysis of RiPSC lines, parental fibroblasts, and hESC controls.

(C) Global gene expression profiles of BJ-, MRC5-, and dH1F-derived RiPSCs shown in scatter plots against parental fibroblasts and hESCs with pluripotency-associated transcripts indicated.

(D) Dendrogram showing unsupervised hierarchical clustering of the global expression profiles for RiPSCs, parental fibroblasts, hESCs, and virus-derived iPSCs.

kinetics of modified RNA iPSC derivation were almost twice as fast as retroviral iPSC derivation. Thus, by the combined criteria of colony numbers and kinetics of reprogramming, the efficiency of modified RNA iPSC derivation greatly exceeds that of conventional retroviral approaches.

It should be noted that in the experiments described above, transfected fibroblast cultures were passaged once at an early time point (day 6 or 7) in order to promote fibroblast proliferation, which has been shown to facilitate reprogramming (Hanna et al., 2009). However, in preliminary experiments, RiPSCs were also efficiently derived from BJ and Detroit 551 fibroblasts in the absence of cell passaging, indicating that splitting the culture during the reprogramming process was not required for modified RNA iPSC derivation (Figure S4, and data not shown).

Utilization of Modified RNA to Direct Differentiation of Pluripotent RiPSCs to a Terminally Differentiated Cell Fate

To realize the promise of iPSC technology for regenerative medicine or disease modeling, it is imperative that the multilineage differentiation potential of pluripotent cells be harnessed. Although progress has been made in directing the differentiation of pluripotent ESCs to various lineages by modulating the extracellular cytokine milieu, such protocols remain relatively

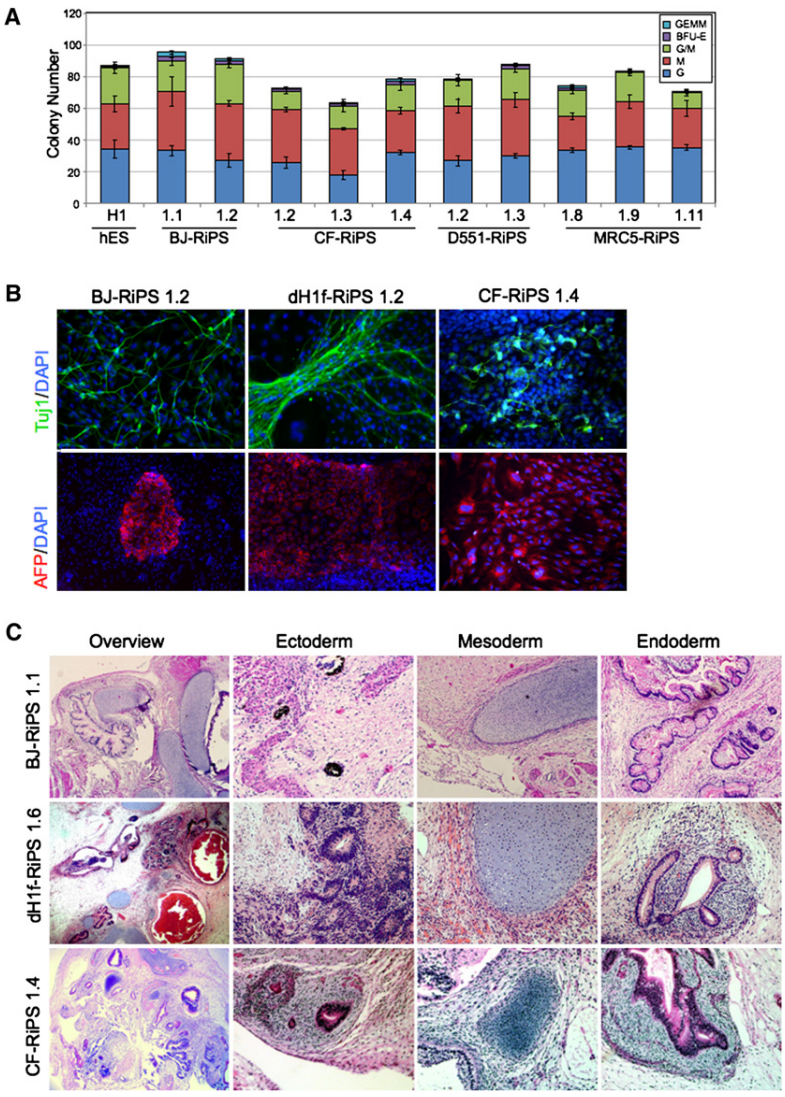

Figure 4. Trilineage Differentiation of RiPSCs

(A) Yield and typology of blood-lineage colonies produced by directed differentiation of embryoid bodies in methylcellulose assays with RiPSC clones derived from BJ, CF, D551, and MCR5 fibroblasts, and a human ESC (H1) control.

(B) Immunostaining showing expression of the lineage markers Tuj1 (neuronal, ectodermal) and alpha-fetoprotein (epithelial, endodermal) in RiPSC clones from three independent RiPSC derivations subjected to directed differentiation.

(C) Hematoxylin and eosin staining of BJ-, CF-, and dH1F-RiPSC-derived teratomas showing histological overview, ectoderm (pigmented epithelia [BJ and CF], neural rosettes [dH1F]), mesoderm (cartilage, all), and endoderm (gut-like endothelium, all). For blood formation and methylcellulose assays, n = 3 for each clone.

See also Figure S5.

inefficient. Given the high efficiency of iPSC derivation by modified RNAs, we reasoned that this technology might also be utilized to redirect pluripotent cells toward differentiated cell fates. To test this hypothesis, we subjected one of our validated RiPSC lines to a simple in vitro differentiation protocol in which FGF was withdrawn, serum added, and the cells plated onto gelatin (Figure 6). Cells obtained under these conditions were then subjected to three consecutive days of transfection with a MYOD-encoding modified RNA followed by an additional 3 days of culture in low serum conditions. The cultures were then fixed and immunostained for the myogenic markers myogenin and MyHC, which revealed a high percentage of large multinucleated myogenin and MyHC double-positive myotubes (Figure 6).

Taken together, these experiments provide proof of principle that modified RNAs can be used to both efficiently reprogram cells to a pluripotent state and direct the fate of such cells to a terminally differentiated somatic cell type.

DISCUSSION

By using a combination of RNA modifications and a soluble interferon inhibitor to overcome innate antiviral responses, we have developed a technology that enables highly efficient reprogramming of somatic cells to pluripotency and can also be harnessed to direct the differentiation of pluripotent cells toward a desired lineage. Although it is relatively technically complex, the methodology described here offers several key advantages over established reprogramming techniques. By obviating the need to perform experiments under the stringent biological containment required for virus-based approaches, modified RNA technology should make reprogramming accessible to a wider community of researchers. More fundamentally, because our technology is RNA based, it completely eliminates the risk of genomic integration and insertional mutagenesis inherent to all DNA-based methodologies, including those that are ostensibly nonintegrating. Moreover, our approach allows protein stoichiometry to be exquisitely regulated within cultures while avoiding the stochastic variation of expression typical of integrating vectors, as well as the uncontrollable effects of viral silencing. Given the stepwise character of the phenotypic changes observed during pluripotency induction (Chan et al., 2009; Smith et al., 2010), it seems likely that individual transcription factors play distinct, stage-specific roles during reprogramming. The unprecedented potential for temporal control over individual factor expression afforded by our technology should help researchers unravel these nuances, yielding insights that can be applied to further enhance the efficiency and kinetics of reprogramming.

The risk of mutagenesis is not the only safety concern holding back clinical application of induced pluripotency, and it has become increasingly apparent that all iPSCs are not created equal with respect to epigenetic landscape and developmental plasticity (Hu et al., 2010; Miura et al., 2009). In this regard, we

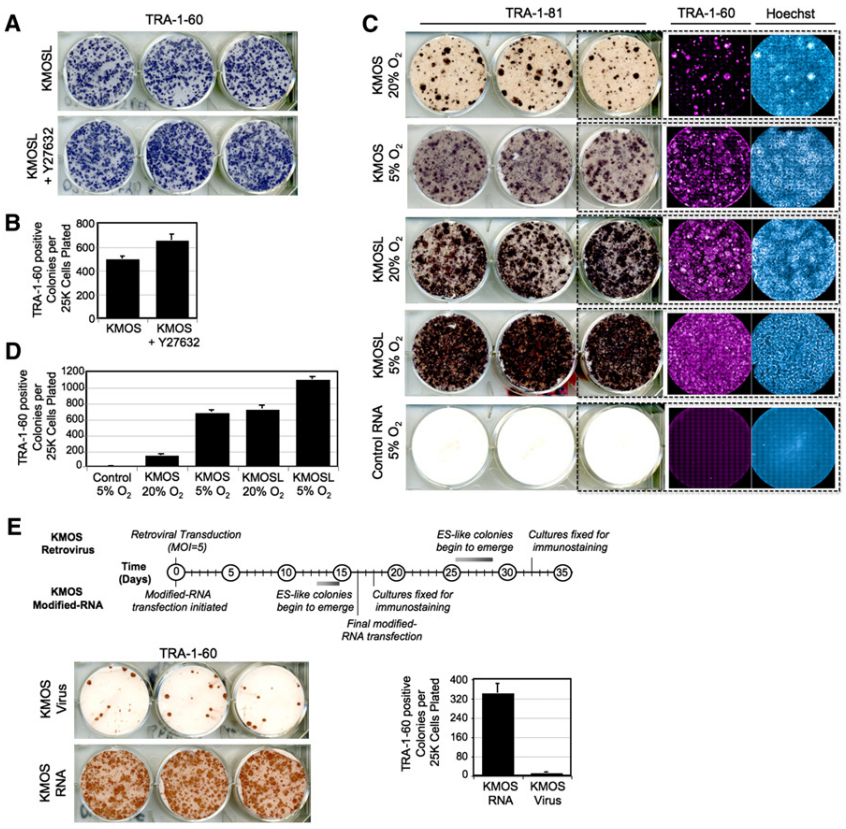

Figure 5. Pluripotency Induction by Modified RNAs Is Highly Efficient

(A and B) TRA-1-60 horseradish peroxidase (HRP) staining conducted at day 18 of a BJ-RiPSC derivation with modified RNAs encoding KMOSL (A) and frequency of TRA-1-60-positive colonies produced in the experiment relative to number of cells initially seeded (B). Error bars show SD, n = 6 for each condition.

(C and D) TRA-181 HRP, TRA-160 immunofluorescence, and Hoechst staining (C) and colony frequencies for dH1f-RiPS experiments done with 4-factor (KMOS) and 5-factor (KMOSL) modified RNA cocktails under 5% O_2 or ambient oxygen culture conditions quantified at day 18 (D). Control wells were transfected with equal doses of modified RNA encoding GFP.

(E) Kinetics and efficiency of retroviral and modified RNA reprogramming. Timeline of colony formation (top), TRA-1-60 HRP immunostaining (bottom left), and TRA-1-60-positive colony counts (bottom right) of dH1f cells reprogrammed with KMOS retroviruses (MOI = 5 of each) or modified RNA KMOS cocktails (n = 3 for each condition).

See also Figure S4.

have applied the most stringent molecular and functional criteria for reprogramming human cells to pluripotency (Chan et al., 2009; Smith et al., 2009). Our results demonstrate that modified RNA-derived iPSC clones from multiple independent derivations were fully reprogrammed to pluripotency and that the resulting cells very closely recapitulated the functional and molecular properties of human ESCs. Our observation that modified RNA-derived iPSCs more faithfully recapitulated the global transcriptional signature of human ESCs than retrovirally derived iPSCs is important because it suggests that RNA reprogramming may produce higher-quality iPSCs, possibly owing to the fact that they are transgene free.

The transient and nonmutagenic character of RNA-based protein expression could also deliver important clinical benefits outside the domain of lineage reprogramming. Indeed, the use of RNA transfection to express cancer or pathogen antigens for immunotherapy is already an active research area (Rabinovich et al., 2006, 2008; Van den Bosch et al., 2006; Weissman et al., 2000), and such approaches may benefit from the nonimmunogenic properties of modified RNAs. One can readily envisage employing modified RNA to transiently express surface proteins such as homing receptors to target cellular therapies toward specific organs, tissues, or diseased cells.

For tissue engineering to progress further into the clinic, there is a pressing need for safe and efficient means to redirect cell fate. This is doubly apparent when one considers that iPSCs are only a starting point for patient-specific therapies, and specification of clinically useful cell types is still required to produce autologous tissues for transplantation or for disease modeling. Importantly, we have demonstrated that our modified RNA-based technology enables highly efficient reprogramming and that it can equally be applied to efficiently redirect pluripotent cell fate to terminally differentiated fates without compromising genomic integrity. In light of these considerations, we believe that our approach has the potential to become a major enabling technology for cell-based therapies and regenerative medicine.

EXPERIMENTAL PROCEDURES

Construction of IVT Templates

The pipeline for production of IVT template constructs and subsequent RNA synthesis is schematized in Figure S1. The oligonucleotide sequences used in the construction of IVT templates are shown in Table S2. All oligos were synthesized by Integrated DNA Technologies (Coralville, IA). ORF PCRs were templated from plasmids bearing human KLF4, c-MYC, OCT4, SOX2, human ESC cDNA (LIN28), Clontech pIRES-eGFP (eGFP), pRVGP (d2eGFP), and CMV-MyoD from Addgene. The ORF of the low-stability nuclear GFP was constructed by combining the d2eGFP ORF with a 3′ nuclear localization sequence. PCR reactions were performed with HiFi Hotstart (KAPA Biosystems, Woburn, MA) per the manufacturer's instructions. Splint-mediated ligations were carried out with Ampligase Thermostable DNA Ligase (Epicenter Biotechnologies, Madison, WI). UTR ligations were conducted in the presence of 200 nM UTR oligos and 100 nM splint oligos, with 5 cycles of the following annealing profile: 95°C for 10 s; 45°C for 1 min; 50°C for 1 min; 55°C for 1 min; 60°C for 1 min. A phosphorylated forward primer was employed in the ORF PCRs to facilitate ligation of the top strand to the 5′ UTR fragment. The 3′ UTR fragment was also 5′-phosphorylated via polynucleotide kinase (New England Biolabs, Ipswich, MA). All intermediate PCR and ligation products were purified with QIAquick spin columns (QIAGEN, Valencia, CA) before further processing. Template PCR amplicons were subcloned with the pcDNA

Table 1. Quantification of Reprogramming Efficiency

Experiment	Cells Plated	Split	Condition	Well Fraction	Colonies/Well	Efficiency (%)
BJ (KMOSL)	300,000	d7	Y27632-	1/24	249 ± 21	2.0
			Y27632+	1/24	326 ± 49	2.6
4-Factor (KMOS) versus 5-Factor (KMOSL)	50,000	d6	4F 20% O_2	1/6	48 ± 18	0.6
			4F 5% O_2	1/6	228 ± 30	2.7
			5F 20% O_2	1/6	243 ± 42	2.9
			5F 5% O_2	1/6	367 ± 38	4.4
RNA versus Virus (KMOS)	100,000	d6	virus	1/3	13 ± 3.5	0.04
			RNA	1/6	229 ± 39	1.4

For each experimental condition, efficiency was calculated by dividing the average count of TRA-1-60-positive colonies per well by the initial number of cells plated, scaled to the fraction of cells replated in each well. Cultures were passaged at day 6 or 7 as indicated. The BJ experiment was started in a 10 cm dish; dH1f trials in individual wells of a 6-well plate. Colony counts are shown ± SD, n = 6, except in the RNA versus Virus trial, where n = 9 for virus, n = 18 for RNA.

3.3-TOPO TA cloning kit (Invitrogen, Carlsbad, CA). Plasmid inserts were excised by restriction digest and recovered with SizeSelect gels (Invitrogen) before being used to template tail PCRs.

Synthesis of Modified RNA

RNA was synthesized with the MEGAscript T7 kit (Ambion, Austin, TX), with 1.6 μg of purified tail PCR product to template each 40 μL reaction. A custom ribonucleoside blend was used comprising 3′-0-Me-m^{7}G(5′)ppp(5′)G ARCA cap analog (New England Biolabs), adenosine triphosphate and guanosine triphosphate (USB, Cleveland, OH), 5-methylcytidine triphosphate and pseudouridine triphosphate (TriLink Biotechnologies, San Diego, CA). Final nucleotide reaction concentrations were 6 mM for the cap analog, 1.5 mM for guanosine triphosphate, and 7.5 mM for the other nucleotides. Reactions were incubated 3–6 hr at 37°C and DNase treated as directed by the manufacturer. RNA was purified with Ambion MEGAclear spin columns, then treated with Antarctic Phosphatase (New England Biolabs) for 30 min at 37°C to remove residual 5′-triphosphates. Treated RNA was repurified, quantitated by Nanodrop (Thermo Scientific, Waltham, MA), and adjusted to 100 ng/μL working concentration by addition of Tris-EDTA (pH 7.0). RNA reprogramming cocktails were prepared by pooling individual 100 ng/μL RNA stocks to produce a 100 ng/μL (total) blend. The KMOS[L]+GFP cocktails were formulated to give equal molarity for each component except for OCT4, which was included at 3× molar concentration. Volumetric ratios used for pooling were as follows: 170:160:420:130:120[:90] (KLF4:c-MYC:OCT4:SOX2:GFP[:LIN28]).

Cells

Primary human neonatal epidermal keratinocytes, BJ human neonatal foreskin fibroblasts, MRC-5 human fetal lung fibroblasts, and Detroit 551 human fetal skin fibroblasts were obtained from ATCC (Manassas, VA). CF cells were obtained with informed consent from a skin biopsy taken from an adult cystic fibrosis patient. dH1f fibroblasts were subcloned from fibroblasts produced by directed differentiation of the H1-OGN human ESC line as previously described (Park et al., 2008). BGO1 hESCs were obtained from BresaGen (Athens, GA). H1 and H9 hESCs were obtained from WiCell (Madison, Wi).

RNA Transfection

RNA transfections were carried out with RNAiMAX (Invitrogen) or TransIT-mRNA (Mirus Bio, Madison, WI) cationic lipid delivery vehicles. RNAiMAX was used for RiPSC derivations, the RiPSC-to-myogenic conversion, and for the multiple cell type transfection experiment documented in Figure S2. All other transfections were performed with TransIT-mRNA. For RNAiMAX transfections, RNA and reagent were first diluted in Opti-MEM basal media (Invitrogen). 100 ng/μL RNA was diluted 5× and 5 μL of RNAiMAX per microgram of RNA was diluted 10×, then these components were pooled and incubated 15 min at room temperature (RT) before being dispensed to culture

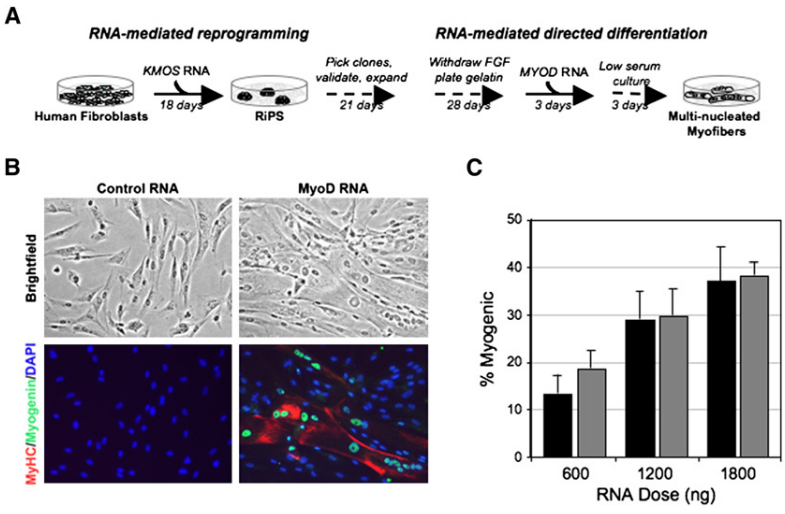

Figure 6. Efficient Directed Differentiation of RiPSCs to Terminally Differentiated Myogenic Fate via Modified RNA

(A) Schematic of experimental design.

(B) Bright-field and immunostained images showing large, multinucleated, myosin heavy chain (MyHC) and myogenin-positive myotubes in cells fixed 3 days after cessation of *MYOD* modified RNA transfection. Modified RNA encoding GFP was administered to the controls.

(C) Penetrance of myogenic conversion relative to daily RNA dose. Black bars refer to an experiment in which cultures were plated at 10^4 cells/cm^2, gray bars to cultures plated at 5 × 10^3 cells/cm^2. Error bars show SD for triplicate wells.

media. For TransIT-mRNA transfections, 100 ng/μL RNA was diluted 10× in Opti-MEM and BOOST reagent was added (2 μL per microgram of RNA), then TransIT-mRNA was added (2 μL per microgram of RNA), and the RNA-lipid complexes were delivered to culture media after a 2 min incubation at RT. RNA transfections were performed in Nutristem xeno-free hESC media (Stemgent, Cambridge, MA) for RiPSC derivations, Dermal Cell Basal Medium plus Keratinocyte Growth Kit (ATCC) for keratinocyte experiments, and Opti-MEM plus 2% FBS for all other experiments described. The B18R interferon inhibitor (eBioscience, San Diego, CA) was used as a media supplement at 200 ng/mL.

qRT-PCR

Transfected cells were lysed with 400 μL CellsDirect reagents (Invitrogen), and 20 μL of each lysate was taken forward to a 50 μL reverse transcription reaction via the VILO cDNA synthesis kit (Invitrogen). Reactions were purified on QIAquick columns (QIAGEN). qRT-PCR reactions were performed with SYBR FAST qPCR supermix (KAPA Biosystems).

Reprogramming to Pluripotency

Gamma-irradiated human neonatal fibroblast feeders (GlobalStem, Rockville, MD) were seeded at 33,000 cells/cm^2. Nutristem media was replaced daily, 4 hr after transfection, and supplemented with 100 ng/mL bFGF and 200 ng/mL B18R (eBioscience, San Diego, CA). Where applied, VPA was added to media at 1 mM final concentration on days 8–15 of reprogramming. Low-oxygen experiments were carried out in a NAPCO 8000 WJ incubator (Thermo Scientific). Media were equilibrated at 5% O_2 for approximately 4 hr before use. Cultures were passaged with TrypLE Select recombinant protease (Invitrogen). Y27632 ROCK inhibitor (Watanabe et al., 2007) was used at 10 μM in recipient plates until the next media change. The daily RNA dose applied in the RiPSC derivations was 1200 ng per well (6-well plate format) or 8 μg to a 10 cm dish.

For RNA versus retrovirus experiments, starting cultures were seeded with 100,000 cells in individual wells of a 6-well plate via fibroblast media (DMEM+10% FBS). The next day (day 1), KMOS RNA transfections were initiated in the RNA plate, and the viral plate was transduced with a KMOS retroviral cocktail (MOI = 5 for each virus). All wells were passaged on day 6, with split ratios of 1:6 for the RNA wells and 1:3 for the virus wells. The conditions applied in the RNA arm of the trial were as in the initial RiPSC derivation, including the use of Nutristem supplemented with 100 ng/mL bFGF, 5% O_2 culture, and human fibroblast feeders. Ambient oxygen tension and other conventional iPSC derivation conditions were used in the viral arm, the cells being grown in fibroblast media without feeders until the day 6 split, then being replated onto CF1 MEF feeders (GlobalStem) with a switch to hESC media based on Knockout Serum Replacement (Invitrogen) supplemented with 10 ng/mL bFGF.

RiPSC Culturing

RiPSC colonies were mechanically picked and transferred to MEF-coated 24-well plates with standard hESC medium containing 5 μM Y27632 (BioMol, Plymouth Meeting, PA). The hESC media comprised DMEM/F12 supplemented with 20% Knockout Serum Replacement (Invitrogen), 10 ng/mL of bFGF (Gembio, West Sacramento, CA), 1× nonessential amino acids (Invitrogen), 0.1 mM β-ME (Sigma), 1 mM L-glutamine (Invitrogen), plus antibiotics. Clones were mechanically passaged once more to MEF-coated 6-well plates, and then expanded via enzymatic passaging with collagenase IV (Invitrogen). For RNA and DNA preparation, cells were plated onto hESC-qualified Matrigel (BD Biosciences) in mTeSR (Stem Cell Technologies, Vancouver, BC) and further expanded by enzymatic passaging with dispase (Stem Cell Technologies).

Immunostaining

Cells were fixed in 4% paraformaldehyde for 20 min. Washed cells were treated with 0.2% Triton X (Sigma) in PBS for 30 min. Cells were blocked with 3% BSA (Invitrogen) and 5% donkey serum (Sigma) for 2 hr at RT. Cells were stained in blocking buffer with primary antibodies at 4°C overnight. Cells were washed and stained with secondary antibodies and 1 μg/mL Hoechst 33342 (Invitrogen) in blocking buffer for 3 hr at 4°C or for 1 hr at RT, protected from light. Antibodies were used, at 1:100 dilution: TRA-1-60-Alexa Fluor 647, TRA-1-81-Alexa Fluor 488, SSEA-4-Alexa Fluor 647, and SSEA-3-Alexa 488 (BD Biosciences). Primary OCT4 and NANOG antibodies (Abcam, Cambridge, MA) were used at 0.5 μg/mL, and an anti-rabbit IgG Alexa Fluor 555 (Invitrogen) was used as the secondary. Images were acquired with a Pathway 435 bioimager (BD Biosciences). Live imaging was performed as described previously (Chan et al., 2009). For pluripotency factor time course experiments, transfected human keratinocytes were trypsinized, washed with PBS, and fixed in 4% paraformaldehyde for 10 min. Fixed cells were washed with 0.1 M glycine, then blocked and permeabilized in PBS/0.5% saponin/1% goat serum (Rockland Immunochemicals, Gilbertsville, PA) for 20 min. Cells were incubated for 1 hr at RT with 1:100 diluted primary antibodies for KLF4, OCT4, and SOX2 (Stemgent), washed, then for 45 min at RT with 1:200-diluted DyLight 488-labeled secondary antibodies (goat anti-mouse IgG+IgM and goat anti-rabbit IgG). Cells were suspended in PBS and analyzed by flow cytometry.

Gene Expression Analysis

RNA was isolated with the RNeasy kit (QIAGEN) according to the manufacturer's instructions. First-strand cDNA was primed with oligo(dT) primers and qPCR was performed with primer sets as described previously (Park et al., 2008), with Brilliant SYBR Green master mix (Stratagene, La Jolla, CA). For the microarray analysis, RNA probes were prepared and hybridized to Human Genome U133 Plus 2.0 oligonucleotide microarrays (Affymetrix, Santa Clara, CA) per the manufacturer's instructions. Arrays were processed by the Coriell Institute Genotyping and Microarray Center (Camden, NJ). Gene expression levels were normalized with the Robust Multichip Average (RMA) algorithm. Hierarchical clustering was performed by means of the Euclidean distance with average linkage method. The similarity metric for comparison between different cell lines is indicated on the height of cluster dendrogram.

Bisulfite Sequencing

DNA was extracted with the DNeasy Blood and Tissue kit (QIAGEN) according to the manufacturer's protocol. Bisulfite treatment of genomic DNA was carried out with EZ DNA Methylation Kit (Zymo Research, Orange, CA) according to the manufacturer's protocol. For pyrosequencing analysis, the bisulfate-treated DNA was first amplified by HotStar Taq Polymerase (QIAGEN) for 45 cycles of (95°C 30 s; 53°C 30 s; 72°C 30 s). The analysis was performed by EpigenDx with the PSQ96HS system according to standard procedures with primers that were developed by EpigenDx for the CpG sites at positions (−50) to (+96) from the start codon of the *OCT4* gene.

Trilineage Differentiation

Embryoid body (EB) hematopoietic differentiation was performed as previously described (Chadwick et al., 2003). In brief, RiPSCs and hESC controls were passaged with collagenase IV and transferred (3:1) in differentiation medium to 6-well low-attachment plates and placed on a shaker in a 37°C incubator overnight. Starting the next day, media was supplemented with the following hematopoietic cytokines: 10 ng/mL of interleukin-3 (R&D Systems, Minneapolis, MN) and interleukin-6 (R&D), 50 ng/mL of G-CSF (Amgen, Thousand Oaks, CA) and BMP-4 (R&D), and 300 ng/mL of SCF (Amgen) and Flt-3 (R&D). Media was changed every 3 days. On day 14 of differentiation, EBs were dissociated with collagenase B (Roche, Indianapolis, IN). 2 × 10^4 differentiated cells were plated into methylcellulose H4434 (Stem Cell Technologies) and transferred with a blunt needle onto 35 mm dishes (Stem Cell Technologies) in triplicate and incubated at 37°C and 5% CO_2 for 14 days. Colony forming units (CFUs) were scored based on morphological characteristics.

For neuronal differentiation, cells were differentiated at 70% confluency as a monolayer in neuronal differentiation medium (DMEM/F12, Glutamax 1%, B27-Supplement 1%, N2-Supplement 2%, P/S 1%, and noggin 20 ng/ml). After 7 days, neuronal structures were visible. For endoderm differentiation (AFP stain), cells were differentiated as a monolayer in endoderm differentiation medium (DMEM, B27(-RA), and 100 ng/ml activin-a) for 7 days, then switched to growth medium (DMEM, 10% FBS, 1% P/S) and continued differentiation for 7 days. Antibodies used were as follows: anti-β-Tubulin III (Tuj1) rabbit anti-human (Sigma, St. Louis, MO), 1:500; AFP (h-140) rabbit polyclonal IgG (Santa Cruz Biotechnology, Santa Cruz, CA), 1:100 dilution. Secondary antibodies were conjugated to Alexa Fluor 488 or Alexa Fluor 594.

For cardiomyocyte differentiation, colonies were digested at 70% confluency with dispase and placed in suspension culture for embryoid body (EB) formation in differentiation medium (DMEM, 15% FBS, 100 μM ascorbic acid). After 11 days, EBs were plated to adherent conditions via gelatin and the same medium. Beating cardiomyocytes were observed 3 days after replating.

For teratomas, 2.5 × 10^6 cells were spun down, and all excess media was removed. In 20-week-old female SCID mice, the capsule of the right kidney was gently elevated, and one droplet of concentrated cells was inserted under the capsule. Tumors harvested at 6–12 weeks were fixed in 4% PFA, run through an ethanol gradient, and stored in 70% ethanol. Specimens were sectioned and stained with H&E.

Myogenic Differentiation of RiPSCs

Validated RiPSCs were plated into wells coated with 0.1% gelatin (Millipore, Billerica, MA) and cultured in DMEM+10% FBS for 4 weeks with passaging every 4–6 days via trypsin. The culture media was switched to Opti-MEM+2% FBS, and the cells were transfected with modified RNA encoding either murine MYOD or GFP the following day, and for the following 2 days. Media was supplemented with B18R and replaced 4 hr after each transfection. After the third and final transfection, the media was switched to DMEM+3% horse serum, and cultures were incubated for a further 3 days. Cells were then fixed in 4% PFA and immunostained as previously described (Shea et al., 2010). The percentage of myogenin-positive nuclei/total nuclei and nuclei/MyHC-positive myotubes was quantified, with a minimum of 500 nuclei counted per condition.

Technical Notes

Although reprogramming and directed differentiation via modified RNAs are efficient processes, the protocols involved are nonetheless multistepped and complex. It is therefore advised that in efforts to apply this methodology, all steps of the protocols described herein are followed rigorously and quality controlled. Foremost among these: templates for RNA synthesis must be sequenced, and production of in vitro transcribed modified RNAs must be quality controlled by gel electrophoresis and spectrophotometry. Critically, the expression of proteins with modified RNAs must be confirmed by immunostaining. Modified RNAs must also be tested for immunogenicity at multiple points throughout the course of the experiment. Successful daily transfection must be monitored by inclusion of modified RNA encoding a fluorescent reporter throughout the course of experiments. Any reagents involved in supporting pluripotency induction (media, feeder cells, etc.) should be tested for their ability to support the growth of pluripotent cells prior to the start of experiments. As is true of reprogramming by other methods, the quality of the starting cells (e.g., passage number) impacts reprogramming via our technology.

ACCESSION NUMBERS

The microarray data are available in the Gene Expression Omnibus (GEO) database (http://www.ncbi.nlm.nih.gov/gds) under the accession number GSE23583.

SUPPLEMENTAL INFORMATION

Supplemental Information includes five figures, three tables, and one movie and can be found with this article online at doi:10.1016/j.stem.2010.08.012.

ACKNOWLEDGMENTS

The authors wish to thank Sun Hur, Victor Li, Laurence Daheron, Odelya Hartung, Alys Peisley, Sutheera Ratanasirintrawoot, Brad Hamilton, Chenmei Luo, Jonathan Kagan, Julie Sahalie, Alejandro De Los Angeles, and Lior Zangi for help, insight, and suggestions. D.J.R., A.M., G.Q.D, A.S.B, C.C., and T.M.S. were supported by grants from the Harvard Stem Cell Institute. Y.-H.L. is supported by the A*Star Institute of Medical Biology and Singapore stem cell consortium. T.A. was supported by the Roberto and Allison Mignone Fund for Stem Cell Research. J.J.C. is supported by Howard Hughes Medical Institute, SysCODE (Systems-based Consortium for Organ Design & Engineering), and NIH grant # RL1DE019021. D.J.R. recently founded a company, ModeRNA Therapeutics, dedicated to the clinical translation of this technology. G.Q.D. is a member of the scientific advisory boards and holds equity in the following companies: Epizyme, iPierian, Solasia KK, and MPM Capital, LLP. C.C. is on the SAB of Ipierian. L.W. is a consultant for Stemgent.

Received: March 30, 2010
Revised: May 11, 2010
Accepted: August 11, 2010
Published online: September 30, 2010

REFERENCES

Audouy, S., and Hoekstra, D. (2001). Cationic lipid-mediated transfection in vitro and in vivo (review). Mol. Membr. Biol. *18*, 129–143.

Chadwick, K., Wang, L., Li, L., Menendez, P., Murdoch, B., Rouleau, A., and Bhatia, M. (2003). Cytokines and BMP-4 promote hematopoietic differentiation of human embryonic stem cells. Blood *102*, 906–915.

Chan, E.M., Ratanasirintrawoot, S., Park, I.H., Manos, P.D., Loh, Y.H., Huo, H., Miller, J.D., Hartung, O., Rho, J., Ince, T.A., et al. (2009). Live cell imaging distinguishes bona fide human iPS cells from partially reprogrammed cells. Nat. Biotechnol. *27*, 1033–1037.

Chang, C.-W., Lai, Y.-S., Pawlik, K.M., Liu, K., Sun, C.-W., Li, C., Schoeb, T.R., and Townes, T.M. (2009). Polycistronic lentiviral vector for "hit and run" reprogramming of adult skin fibroblasts to induced pluripotent stem cells. Stem Cells *27*, 1042–1049.

Davis, R.L., Weintraub, H., and Lassar, A.B. (1987). Expression of a single transfected cDNA converts fibroblasts to myoblasts. Cell *51*, 987–1000.

Diebold, S.S., Kaisho, T., Hemmi, H., Akira, S., and Reis e Sousa, C. (2004). Innate antiviral responses by means of TLR7-mediated recognition of single-stranded RNA. Science *303*, 1529–1531.

Elango, N., Elango, S., Shivshankar, P., and Katz, M.S. (2005). Optimized transfection of mRNA transcribed from a d(A/T)100 tail-containing vector. Biochem. Biophys. Res. Commun. *330*, 958–966.

Fusaki, N., Ban, H., Nishiyama, A., Saeki, K., and Hasegawa, M. (2009). Efficient induction of transgene-free human pluripotent stem cells using a vector based on Sendai virus, an RNA virus that does not integrate into the host genome. Proc. Jpn. Acad., Ser. B, Phys. Biol. Sci. *85*, 348–362.

Hanna, J., Saha, K., Pando, B., van Zon, J., Lengner, C.J., Creyghton, M.P., van Oudenaarden, A., and Jaenisch, R. (2009). Direct cell reprogramming is a stochastic process amenable to acceleration. Nature *462*, 595–601.

Holtkamp, S., Kreiter, S., Selmi, A., Simon, P., Koslowski, M., Huber, C., Türeci, O., and Sahin, U. (2006). Modification of antigen-encoding RNA increases stability, translational efficacy, and T-cell stimulatory capacity of dendritic cells. Blood *108*, 4009–4017.

Hornung, V., Ellegast, J., Kim, S., Brzózka, K., Jung, A., Kato, H., Poeck, H., Akira, S., Conzelmann, K.-K., Schlee, M., et al. (2006). 5′-Triphosphate RNA is the ligand for RIG-I. Science *314*, 994–997.

Hu, B.Y., Weick, J.P., Yu, J., Ma, L.X., Zhang, X.Q., Thomson, J.A., and Zhang, S.C. (2010). Neural differentiation of human induced pluripotent stem cells follows developmental principles but with variable potency. Proc. Natl. Acad. Sci. USA *107*, 4335–4340.

Huangfu, D., Maehr, R., Guo, W., Eijkelenboom, A., Snitow, M., Chen, A.E., and Melton, D.A. (2008). Induction of pluripotent stem cells by defined factors is greatly improved by small-molecule compounds. Nat. Biotechnol. *26*, 795–797.

Jia, F., Wilson, K.D., Sun, N., Gupta, D.M., Huang, M., Li, Z., Panetta, N.J., Chen, Z.Y., Robbins, R.C., Kay, M.A., et al. (2010). A nonviral minicircle vector for deriving human iPS cells. Nat. Methods *7*, 197–199.

Kaji, K., Norrby, K., Paca, A., Mileikovsky, M., Mohseni, P., and Woltjen, K. (2009). Virus-free induction of pluripotency and subsequent excision of reprogramming factors. Nature *458*, 771–775.

Karikó, K., and Weissman, D. (2007). Naturally occurring nucleoside modifications suppress the immunostimulatory activity of RNA: implication for therapeutic RNA development. Curr. Opin. Drug Discov. Devel. *10*, 523–532.

Karikó, K., Buckstein, M., Ni, H., and Weissman, D. (2005). Suppression of RNA recognition by Toll-like receptors: The impact of nucleoside modification and the evolutionary origin of RNA. Immunity *23*, 165–175.

Karikó, K., Muramatsu, H., Welsh, F.A., Ludwig, J., Kato, H., Akira, S., and Weissman, D. (2008). Incorporation of pseudouridine into mRNA yields superior nonimmunogenic vector with increased translational capacity and biological stability. Mol. Ther. *16*, 1833–1840.

Kawai, T., and Akira, S. (2007). Antiviral signaling through pattern recognition receptors. J. Biochem. *141*, 137–145.

Kawamura, T., Suzuki, J., Wang, Y.V., Menendez, S., Morera, L.B., Raya, A., Wahl, G.M., and Belmonte, J.C. (2009). Linking the p53 tumour suppressor pathway to somatic cell reprogramming. Nature *460*, 1140–1144.

Kim, D., Kim, C.-H., Moon, J.-I., Chung, Y.-G., Chang, M.-Y., Han, B.-S., Ko, S., Yang, E., Cha, K.Y., Lanza, R., and Kim, K.S. (2009). Generation of human induced pluripotent stem cells by direct delivery of reprogramming proteins. Cell Stem Cell *4*, 472–476.

Li, X., Zhao, X., Fang, Y., Jiang, X., Duong, T., Fan, C., Huang, C.-C., and Kain, S.R. (1998). Generation of destabilized green fluorescent protein as a transcription reporter. J. Biol. Chem. *273*, 34970–34975.

Lowry, W.E., Richter, L., Yachechko, R., Pyle, A.D., Tchieu, J., Sridharan, R., Clark, A.T., and Plath, K. (2008). Generation of human induced pluripotent stem cells from dermal fibroblasts. Proc. Natl. Acad. Sci. USA *105*, 2883–2888.

Miura, K., Okada, Y., Aoi, T., Okada, A., Takahashi, K., Okita, K., Nakagawa, M., Koyanagi, M., Tanabe, K., Ohnuki, M., et al. (2009). Variation in the safety of induced pluripotent stem cell lines. Nat. Biotechnol. *27*, 743–745.

Nallagatla, S.R., and Bevilacqua, P.C. (2008). Nucleoside modifications modulate activation of the protein kinase PKR in an RNA structure-specific manner. RNA *14*, 1201–1213.

Nallagatla, S.R., Toroney, R., and Bevilacqua, P.C. (2008). A brilliant disguise for self RNA: 5′-end and internal modifications of primary transcripts suppress elements of innate immunity. RNA Biol. *5*, 140–144.

Okita, K., Nakagawa, M., Hyenjong, H., Ichisaka, T., and Yamanaka, S. (2008). Generation of mouse induced pluripotent stem cells without viral vectors. Science *322*, 949–953.

Papapetrou, E.P., Tomishima, M.J., Chambers, S.M., Mica, Y., Reed, E., Menon, J., Tabar, V., Mo, Q., Studer, L., and Sadelain, M. (2009). Stoichiometric and temporal requirements of Oct4, Sox2, Klf4, and c-Myc expression for efficient human iPSC induction and differentiation. Proc. Natl. Acad. Sci. USA *106*, 12759–12764.

Park, I.-H., Zhao, R., West, J.A., Yabuuchi, A., Huo, H., Ince, T.A., Lerou, P.H., Lensch, M.W., and Daley, G.Q. (2008). Reprogramming of human somatic cells to pluripotency with defined factors. Nature *451*, 141–146.

Pichlmair, A., Schulz, O., Tan, C.P., Näslund, T.I., Liljeström, P., Weber, F., and Reis e Sousa, C. (2006). RIG-I-mediated antiviral responses to single-stranded RNA bearing 5′-phosphates. Science *314*, 997–1001.

Rabinovich, P.M., Komarovskaya, M.E., Ye, Z.J., Imai, C., Campana, D., Bahceci, E., and Weissman, S.M. (2006). Synthetic messenger RNA as a tool for gene therapy. Hum. Gene Ther. *17*, 1027–1035.

Rabinovich, P.M., Komarovskaya, M.E., Wrzesinski, S.H., Alderman, J.L., Budak-Alpdogan, T., Karpikov, A., Guo, H., Flavell, R.A., Cheung, N.K., Weissman, S.M., and Bahceci, E. (2008). Chimeric receptor mRNA transfection as a tool to generate antineoplastic lymphocytes. Hum. Gene Ther. *20*, 51–61.

Randall, R.E., and Goodbourn, S. (2008). Interferons and viruses: An interplay between induction, signalling, antiviral responses and virus countermeasures. J. Gen. Virol. *89*, 1–47.

Shea, K.L., Xiang, W., LaPorta, V.S., Licht, J.D., Keller, C., Basson, M.A., and Brack, A.S. (2010). Sprouty1 regulates reversible quiescence of a self-renewing adult muscle stem cell pool during regeneration. Cell Stem Cell *6*, 117–129.

Smith, K.P., Luong, M.X., and Stein, G.S. (2009). Pluripotency: Toward a gold standard for human ES and iPS cells. J. Cell. Physiol. *220*, 21–29.

Smith, Z.D., Nachman, I., Regev, A., and Meissner, A. (2010). Dynamic single-cell imaging of direct reprogramming reveals an early specifying event. Nat. Biotechnol. *28*, 521–526.

Stadtfeld, M., Nagaya, M., Utikal, J., Weir, G., and Hochedlinger, K. (2008). Induced pluripotent stem cells generated without viral integration. Science *322*, 945–949.

Symons, J.A., Alcamí, A., and Smith, G.L. (1995). Vaccinia virus encodes a soluble type I interferon receptor of novel structure and broad species specificity. Cell *81*, 551–560.

Takahashi, K., and Yamanaka, S. (2006). Induction of pluripotent stem cells from mouse embryonic and adult fibroblast cultures by defined factors. Cell *126*, 663–676.

Takahashi, K., Tanabe, K., Ohnuki, M., Narita, M., Ichisaka, T., Tomoda, K., and Yamanaka, S. (2007). Induction of pluripotent stem cells from adult human fibroblasts by defined factors. Cell *131*, 861–872.

Uematsu, S., and Akira, S. (2007). Toll-like receptors and Type I interferons. J. Biol. Chem. *282*, 15319–15323.

Utikal, J., Polo, J.M., Stadtfeld, M., Maherali, N., Kulalert, W., Walsh, R.M., Khalil, A., Rheinwald, J.G., and Hochedlinger, K. (2009). Immortalization eliminates a roadblock during cellular reprogramming into iPS cells. Nature *460*, 1145–1148.

Uzri, D., and Gehrke, L. (2009). Nucleotide sequences and modifications that determine RIG-I/RNA binding and signaling activities. J. Virol. *83*, 4174–4184.

Van den Bosch, G.A., Van Gulck, E., Ponsaerts, P., Nijs, G., Lenjou, M., Apers, L., Kint, I., Heyndrickx, L., Vanham, G., Van Bockstaele, D.R., et al. (2006). Simultaneous activation of viral antigen-specific memory CD4+ and CD8+ T-cells using mRNA-electroporated CD40-activated autologous B-cells. J. Immunother. *29*, 512–523.

Van Tendeloo, V.F., Ponsaerts, P., Lardon, F., Nijs, G., Lenjou, M., Van Broeckhoven, C., Van Bockstaele, D.R., and Berneman, Z.N. (2001). Highly efficient gene delivery by mRNA electroporation in human hematopoietic cells: Superiority to lipofection and passive pulsing of mRNA and to electroporation of plasmid cDNA for tumor antigen loading of dendritic cells. Blood *98*, 49–56.

Watanabe, K., Ueno, M., Kamiya, D., Nishiyama, A., Matsumura, M., Wataya, T., Takahashi, J.B., Nishikawa, S., Nishikawa, S.-i., Muguruma, K., and Sasai, Y. (2007). A ROCK inhibitor permits survival of dissociated human embryonic stem cells. Nat. Biotechnol. *25*, 681–686.

Weissman, D., Ni, H., Scales, D., Dude, A., Capodici, J., McGibney, K., Abdool, A., Isaacs, S.N., Cannon, G., and Karikó, K. (2000). HIV gag mRNA transfection of dendritic cells (DC) delivers encoded antigen to MHC class I and II molecules, causes DC maturation, and induces a potent human in vitro primary immune response. J. Immunol. *165*, 4710–4717.

Woltjen, K., Michael, I.P., Mohseni, P., Desai, R., Mileikovsky, M., Hämäläinen, R., Cowling, R., Wang, W., Liu, P., Gertsenstein, M., et al. (2009). piggyBac transposition reprograms fibroblasts to induced pluripotent stem cells. Nature *458*, 766–770.

Yisraeli, J.K., and Melton, D.A. (1989). Synthesis of long, capped transcripts in vitro by SP6 and T7 RNA polymerases. Methods Enzymol. *180*, 42–50.

Yoshida, Y., Takahashi, K., Okita, K., Ichisaka, T., and Yamanaka, S. (2009). Hypoxia enhances the generation of induced pluripotent stem cells. Cell Stem Cell *5*, 237–241.

Yu, J., Vodyanik, M.A., Smuga-Otto, K., Antosiewicz-Bourget, J., Frane, J.L., Tian, S., Nie, J., Jonsdottir, G.A., Ruotti, V., Stewart, R., et al. (2007). Induced pluripotent stem cell lines derived from human somatic cells. Science *318*, 1917–1920.

Yu, J., Hu, K., Smuga-Otto, K., Tian, S., Stewart, R., Slukvin, I.I., and Thomson, J.A. (2009). Human induced pluripotent stem cells free of vector and transgene sequences. Science *324*, 797–801.

Zhou, H., Wu, S., Joo, J.Y., Zhu, S., Han, D.W., Lin, T., Trauger, S., Bien, G., Yao, S., Zhu, Y., et al. (2009). Generation of induced pluripotent stem cells using recombinant proteins. Cell Stem Cell *4*, 381–384.